Journal of High Energy Astrophysics 43 (2024) 79–92

Contents lists available at ScienceDirect

Journal of High Energy Astrophysics

journal homepage: www.elsevier.com/locate/jheap

Accretion flow dynamics and characteristics of MAXI J153–571-spectral analysis using combination of XSPEC and TCAF models

Ambrose C. EZE[a,*], Romanus N.C. EZE[b], Augustine E. CHUKWUDE[b]

[a] Department of Physics and Geosciences, Faculty of Natural Sciences and Environmental Studies, Godfrey Okoye University, Enugu, Nigeria
[b] Department of Physics and Astronomy, Faculty of Physical Sciences, University of Nigeria, Nsukka, Nigeria

ARTICLE INFO

Keywords:
Black hole candidate: MAXI J153–571
Utburst, Accretion flow
Hard X-rays
Spectral and temporal characteristics

ABSTRACT

MAXI J153–571 accretion flow consists of Keplerian (optically thick) and sub-Keplerian (optically thin) flow, and their mass accretion rates seem to regulate other accretion flow characteristics. Hard X-rays are produced when the Keplerian seed soft photons are thermally or inverse comptonized in the Compton cloud/post-shock region by hot electrons. The variations/fluctuations of components of the accretion flow during the hard states create propagating Quasi-periodic oscillation (QPO) when their timescales are roughly matched and resonance phenomena occur. The QPO and its frequency are timing properties and the accretion flow spectra-temporal characteristics can be determined via spectral analysis. In this study, we looked into the accretion flow characteristics of MAXI J153–571 during the hard-intermediate state. Spectral analysis of MAXI J153–571 observed by *MAXI/GSC, Swift/BAT,* and *NuSTAR* on the same or close-in epochs was carried out. *XSPEC* and *TCAF* models were used in fitting/modeling the data. A robust and statistically acceptable fit spectra with a reduced Chi-squared value of $\sim$ 0.84 – 1.20 and best-fit photon index of 2.0–2.29 was obtained. The track of the accretion flow characteristics was obtained using models'–fitted parameters and MATLAB written codes of physical equations. Some accretion flow characteristics are positively correlated while others are anti-correlated at different phases and their correlation are statistically significant. The correlation of accretion flow characteristics with one another suggests that saturation effects, variation/fluctuations in the accretion flow, and intermittent/flickering behavior of MAXI J153–571 are tied to the variations/fluctuations of the intrinsic properties; mass accretion rates. Moreover, a resonance condition of 0.70 to 0.83 indicates that the cooling and infall timescales are roughly matched and affirms the presence of QPO in the accretion flow. This suggests that the origin of the photon index–QPO frequency (Γ–vQPO) relation is strongly linked to the variation/fluctuations in mass accretion flow rates. Hence, the accretion flow is dynamic, and independent variations/fluctuations of mass accretion rates could regulate the variation/fluctuations of other accretion flow parameters and perhaps, spectral evolution.

1. Introduction

Transient outbursts in Low Mass X-ray black hole binaries (LMXBHBs) are triggered by thermal, viscous, and radiative instabilities (Mineshige and Wheeler, 1989). These instabilities are initiated and mediated by the continuous mass accretion from the companion star on timescales (mass accretion rates) onto the black hole (Trudolyubov et al., 1998). The outburst disrupts the accretion disk, and advection and radiative processes cause the accretion flow to evolve (Chakrabarti and Titarchuk, 1995). The truncated disk model infers that the accretion flow consists of optically thin and optically thick plasma. However, the Two-component Advection Flow (TCAF) model presumes these components of the accretion flow to be sub-Keplerian flow and Keplerian flow respectively. The emitted seed soft X-ray photons from the Keplerian region (Ebisawa et al., 1991; Gierlinaski et al., 1999) are conveyed via buoyancy, turbulent convective motion, and magnetic activities (Galeev et al., 1979) to the Compton cloud/post-shock region for interception and thermal or inverse comptonization by hot electrons. This leads to the production of hard X-rays. The truncated disk model and the *TCAF* model consistently explain the comptonization processes in the hard spectral states of BHCs (Hua and Titarchuk, 1995; Laurent and Titarchuk, 1999; Done et al., 2007). Strong coronal and flaring activities are evidenced during the hard states and the accretion flow is mostly advection-dominated and inefficiently radiated (Chakrabarti and

* Corresponding author.
E-mail address: ceze@gouni.edu.ng (A.C. EZE).

https://doi.org/10.1016/j.jheap.2024.06.007
Received 1 March 2024; Received in revised form 20 June 2024; Accepted 20 June 2024
Available online 22 June 2024

Titarchuk, 1995; Beloborodov, 1998; Esin et al., 1998). The produced hard X-ray photons are intercepted by the gradual manifestation of Keplerian flow (optically thick plasma), of which a part of it is absorbed, thermalized, reflected, and re-radiated as soft X-ray photons. These processes repeat and soft X-ray photons are supplied concurrently to the Compton cloud or CENBOL (CENtrifugal pressure supported BOundary Layer; Debnath et al., 2014) via magnetic field/Coulomb coupling (references therein). This dilutes and cools the heating mechanism in the Compton cloud/post-shock (Chakrabarti and Titarchuk, 1995). As a result, the softening of the hardness of the X-ray spectrum ensues and this causes spectral evolution and variation of the power-law photon index (Laurent and Titarchuk, 1999; Remillard and McClintock, 2006). Spectral evolution is regulated by the variations of components of the accretion flow (Homan and Belloni, 2005).

1.1. Accretion flow characteristics of BHBs/BHCs

Accretion flow characteristics (spectral and timing/temporal) solely depend on the evolution of components of the accretion flow (Kubota and Makishima, 2004; Remillard and McClintock, 2006; Chakrabarti and Mandal, 2006; Done et al., 2007). Hard, intermediate, and soft spectral states believed to be initiated and mediated by mass accretion rate variations (Narayan et al., 1995) have been identified in black hole candidates (BHC; Belloni, 2009). The hard state (HS) and soft state (SS) are the two extreme spectral states characterized by non-thermal and multi-color disk blackbody radiations respectively. The intermediate state (IMS: hard-intermediate; HIMS and soft-intermediate; SIMS) is the intermittent, short-lived, and transitory epochs in between the HS and SS (references therein). The hard-to-soft state transition is associated with variations in the power-law photon index from lower to higher values. The power-law photon index varies in the range of $1.3 \leq \Gamma \leq 1.8$, ~ 1.8 to 2.3, and 2.3–3.0 during the HS, HIMS, and SIMS respectively (Esin et al., 1997; Esin et al., 1998; Remillard and McClintock, 2006; Nandi et al., 2012). In the SS, however, the power-law photon index is not often constrained due to the prominence of the thermal-component radiations in the accretion flow (Tanaka and Shibazaki, 1996; Homan and Belloni, 2005). The X-ray spectral and temporal characteristics of BHBs/BHCs are strongly related to each other, and they originate from the variations of components of the accretion flow (Homan and Belloni, 2005). The indicator of changes in the spectral states is Quasi-periodic oscillations (QPOs; Mereminskiy et al., 2018) with a frequency range of 1mHz to 1 kHz (Miyamoto et al., 1991). There is a wide belief that QPO originates from the oscillation of shock waves in the accretion flow (Ryu et al., 1997; Iyer et al., 2015). QPOs are categorized into type –A, –B, and –C, and their frequency is the most important parameter among the temporal characteristics. Type–A QPO is rare, but if seen, appears in the SIMS and/or SS when the fractional root mean square (rms) variability is ≤ 5 %. Type–B QPO is seen in the SIMS when the fractional rms variability is ≈ 5 %–10 % (Méndez and van der Klis, 1997). Moreover, Type–C QPO is seen in the HS and HIMS when the fractional rms variability is $\approx$30–40 % and $\sim$10–30 % respectively. Type–C exhibits strong flat-top noise with frequency in the range of 0.1–10 Hz (Casella et al., 2004; Motta et al., 2012).

1.2. MAXI J1535–571

The outburst of MAXI J1535–571 was detected by Monitor of All-sky X-ray Image/Gas slit camera (MAXI/GSC) on 02 September 2017 at R. A. $= 15^h\ 35^m\ 19.73^s$ and Dec $= -57^\circ\ 13'\ 48''$ (Negoro et al., 2017a, b). *MAXI/GSC, Swift/BAT* (Swift/Burst Alert Telescope), and *NuSTAR (*Nuclear Spectroscopic Telescope Array Mission*)*, monitored MAXI J1535–571 simultaneously (Xu et al., 2018; Nakahira et al., 2018; Tao et al., 2018). MAXI J1535–571 exhibited enormous brightness and X-ray flux variability before it transitioned to the soft spectral state (Tao et al., 2018) where it stayed for a few days. Later, it entered a declining phase probably when the magnetic viscosity dropped and sub-Keplerian flow (optically thin plasma) gradually manifested (Narayan et al., 1995). Two distinct "echoes" (re-flare/re-brightenings) of the main outburst on MJD 58,017 and MJD 58,019 during the SIMS (2017 September 21 and 23) have been reported (Nakahira et al., 2018; Parikh et al., 2018, 2019; Chauhan et al., 2019; Cuneo et al., 2020). MAXI J1535–571 spectral evolution is strongly linked to variations/fluctuation in the mass accretion flow rate (Tao et al., 2018; Nakahira et al., 2018; Sreehari et al., 2019). The time-evolution of components of accretion flow rates ($m_{dot}d$ and $m_{dot}h$ versus MJD) has been portrayed by Shang et al. (2019), but the track of variations of the sub-Keplerian mass accretion rate ($m_{dot}h$) to that of the Keplerian ($m_{dot}d$) on the same and/or close-in epochs have not been elucidated. Furthermore, the presence of QPOs in the accretion flow, as has been seen in other BHCs, is produced either due to non-satisfaction of the Rankine-Hugoniot condition in the SIMS and SS or resonance of propagating oscillatory waves in the post-shock region (Molteni et al., 1995; Ryu et al., 1997). The resonance happens when the infall timescale (of the sub-Keplerian; optically thin plasma) and cooling timescale (of the Keplerian; optically thick plasma) are comparable or match (Mandal and Chakrabarti, 2010). Type-C QPO is a signature of such phenomena in the HS and HIMS of MAXI J1535–571 (Chakrabarti, 2015; Mereminskiy et al., 2018; Stiele and Kong, 2018) and its frequency (of type-C QPO) can be estimated empirically if the oscillating shock is strong (Debnath et al., 2014). The oscillating shock is strong when the shock location/strength is $\geq 38\ r_g$ and the compression ratio (R) and the polytropic index (adiabatic flow constant) of the flow/gas is 4 and 5/3 or 7 and 4/3 respectively (Chakrabarti and Manickam, 2000). The mechanism responsible for the oscillation of waves in the post-shock region of the accretion flow is an open debate. Also, the physical mechanism (s) responsible for (i) the origin of photon index (Γ)–QPO frequency (vQPO) relation, (ii) fluctuations and saturation effect seen in the power-law photon index (Mereminskiy et al., 2018; Bhargava et al., 2019) and X-ray flux variability and flickering behavior of MAXI J1535–571 is ongoing.

In this paper, the spectral analysis of MAXI J1535–571 data observed by three X-ray missions (*MAXI/GSC, Swift/BAT*, and *NuSTAR*) on 2017 September 14, was carried out to elucidate the track of accretion flow characteristics and explain the origin of some physical phenomena. Section 2 is about data acquisition and reduction. Spectral analysis and results are presented in Section 3 whereas Section 4 is the discussion and conclusion. Besides, it is worth noting that we are submitting another manuscript/paper on spectral analysis of MAXI J1535-571 to elucidate the origin of power-law photon index–Quasi-Periodic Oscillation frequency (Γ–vQPO) relation.

2. Data acquisition and reduction

The HEASARC (High Energy Astrophysics Science Archive Research Center) retrieved archival dataset of MAXI J1535–571 observed on the same and/or close-in epochs of 2017 September 14 by *MAXI/GSC, NuSTAR*, and *Swift/BAT* were utilized. The observations were performed at UT 8:36:00 to 21:00:00 (*MAXI/GSC*), UT 20:43:54 to 20:52:58 (Swift/BAT), UT 13:16:09 to 20:16:09 (*NuSTAR*) respectively. HEASoft (High Energy Astrophysical Software) version 6.28 and its software packages, Flexible Image Transport System Tools (*FTOOLS*), and standard pipeline product software of each satellite; *mxproduct (MAXI/GSC), batsurvey product (Swift/BAT), nupipeline* version 1.6 *(NuSTAR)*, were used for data reduction. These detectors' standard pipeline product software was downloaded and set up/included as part of HEASoft 6.28 installed in the Ubuntu 18.04 Operating System. The time-averaged spectra of MAXI J1535–571 observed by the *MAXI/GSC* detector were obtained from the *ondemand* web interface. A circular region of 100–and 180–arc-minute radii were used to extract the MAXI J1535–571 spectrum and background spectrum respectively. While extraction, a proactive measure was taken to ensure that the circular region covers more than 90% of the source's flux and the background extraction was done in a blank-free sky proximity to it. The background spectrum was subtracted from the source spectrum and data.pha file was generated. Moreover, *batsurvey* alongside the 2017 October 16 *Swift/BAT CALDB* software version was used for the reduction of *Swift/BAT* events, and *make_survey_pha script* was used to create source.pha (time-averaged spectra) and source.rsp (response) files. Furthermore, for *NuSTAR*, a circular region of 80 arc-minute radius centered at the source position and 140 arc-minute radius in a source-free area was used for MAXI J1535–571 spectrum and background spectrum extraction respectively. Thereafter, *nuproducts* were used to create source.pha (time-averaged spectra) and source.rsp (response) files after reprocessing the *NuSTAR* events/data with *nustardas_06072017_v1.8.0* and the 2017 August 17 *NuSTAR CALDB* software version.

3.0. Spectral analysis and results

3.1. Spectral analysis

Multi-mission X-ray data analysis software; *XSPEC* version 12.10.1f, was used for spectral analysis. The three detectors' reduced data were fitted and modelled simultaneously. The *XSPEC ignore* command was used to remove the energy bands where there is a low signal-to-noise data ratio. The data within 15–90 keV, 3–8 keV, and 3–60 keV energy bands were used for *Swift/BAT, MAXI/GSC,* and *NuSTAR/FPMA* satellite respectively. The MAXI J1535–571 data was modelled with the selected *XSPEC* model; *tbabs*(bmc*highecut+diskbb)*. The *tbabs* model gives the interstellar absorption of hydrogen density (N_H). The bulk motion comptonization (*bmc)* model explains the non-thermal (power-law) component radiation of the accretion flow and consistently reveals the comptonization of seed soft photons by bulk motion of hot keV electrons (Titarchuk et al., 1997; Borozdin et al., 1999). The *bmc* model alongside the narrow G*aussian* line can be used in modelling the hard spectra (HS and HIMS) of BHCs (Vignarca et al., 2003; Titarchuk et al., 2007). The essence of including the *bmc* model was to determine the saturation effect in the photon index–normalization parameter (which is proportional to the optically thick mass accretion rate; see Fig. 2). The *highecut* model gives the cut-off and e-fold energy of the electron. The *diskbb* model is the multi-color blackbody accretion disk model (Mitsuda et al., 1984) that explains the thermal component radiation of the accretion flow. The *diskbb* model gives the effective temperature and radius of the accretion disk/optically thick plasma. Fitting/modelling the data with the above-combined models gives a reduced Chi-squared value of 6.39 (2960.91/463), and we observed that the power-law spectral index (α) of the *bmc* model is above 1.0 (Titarchuk and Zannias, 1998). This prompted us to add the blackbody (*bbody*) radiation model to suppress the spectral index to ≤ 1.0 such that the power-law photon index $(\alpha + 1)$ required for the HIMS be ≤ 2.0. This improved the statistical fit with a reduced Chi-squared value of 1.32 (608.71/461). The significance of the additional component model was checked by performing the *XSPEC* F-statistics test. The F-test value of 890.707 with a probability of 4.39638×10^{-159} was obtained. The obtained reduced Chi-squared value is greater than the acceptable limit ≤ 1.2. Besides, there is a gross formalism associated with the *diskbb* model (Kubota et al., 1998), and the correlation of estimated optically thick– and optically thin–mass accretion rates we obtained via non-relativistic approximation is absurd. Given this, the general relativistic accretion disk (*grad*) model was added to correct the *diskbb* gross formalism and also to constrain the inclination angle, distance, and mass of the sources as well as the optically thick mass accretion flow rate, even though *diskbb* and *grad* models explain the thermal component radiations of the accretion flow. The statistical fit becomes worse with a reduced Ch-squared value of 1.48. This informed our decision to "thaw" and "steppar" the distance and angle of inclination of the source to see if the fit statistics would improve. As a result, a reduced Chi-squared value of 1.20 (549.89/456) was obtained. The F-statistics test was repeated after adding *grad* model to ascertain its significance, and an F-test value of 9.75538 and probability of 7.21304 $\times 10^{-09}$ was obtained. Later, the narrow Gaussian (*gaus*) iron emission line of 6.5 keV was added to explain the excess X-ray emission or reflection above the accretion disk. This improved the statistical fit with a reduced Chi-squared value of 1.17(533.37/455). The F-test value of 14.0927 (with probability 1.96568×10^{-09}) was obtained. Hence, the composite model; *tbabs*(bmc*highecut+diskbb+bbody+grad+gaus)*, is hereby referred to as "*M1*". A best-fit spectral index of 0.68 (photon index = 1.68) was obtained. This is not the real power-law photon index because the spectral index of the *bmc* model was suppressed. As a result, we explored the option of using other phenomenological models, and the data was modelled again using the two-component comptonization (*nthcomp*) model (Zycki et al., 1999) alongside *diskbb* model; *tbabs* (nthcomp+diskbb)*. This gives a best-fit photon index of 2.2 and a reduced Chi-squared value of 1.46(682.17/465). Thereafter, the data was modelled again by adding *grad* model based on the aforementioned reasons and to see if the fit statistics will improve. A reduced Chi-squared value of 1.39(641.02/460) indicates an improve in statistical fit though this is above the acceptable limit. As a result, the data was modelled again by adding a *gaus* model, and the fit statistic improved with reduced a Chi-squared value of 1.16 (531.38/457). While fitting/modeling the data, the seed soft photon temperature of the *nthcomp* model was "thawed" and tied to the accretion disk temperature so that they be the same or equivalent to represent the temperature of the optically thick plasma. The F-statistics test was repeated when the respective *grad*– and G*aus*–model was added one after the other. The F-test value/probability in each is $5.91164/2.60738 \times 10^{-05}$ and $31.431/ 1.73224 \times 10^{-18}$ respectively. The combined model; *tbabs* (nthcomp+diskbb+grad+gaus),* is hereby referred to as "*M2*". Moreover, the data was modelled again using the power-law dense matter absorption model (Yaqoob, 1997) alongside *diskbb* model; (*PL+diskbb*) to further checkmate the consistency of other models reproducing the power-law photon index. This gives an unacceptable spectral fit-statistic with a reduced Chi-squared value of 1.56 (736.06/ 465). The *grad* model followed by the *gaus* model was added one after the other and the fit-statistic improved with a reduced Chi-squared value of 1.16 (534.10/460) and 1.12 (515.09/457) respectively. The best-fit power--law photon index of 2.1 was obtained. The F-statistics test was repeated as we did in "*M2*" and the F-test value/probability in each case is $34.7881/3.55307 \times 10^{-30}$ and $5.62204/8.61995 \times 10^{-9}$. The composite model; (*PL+diskbb+grad+gaus*), is hereby referred to as "*M3*". Moreover, the fluctuations in the photon index are associated with fluctuations in the Compton temperature (electron temperature; kT_e) and the optical depth (τ_o; Sunyaev and Truemper, 1979). The fluctuations in kT_e and τ_o are believed to be caused by the gradual increase in the intercepted seed soft photons and their thermal or inverse comptonization on timescales (Esin et al., 1998). The photon index (Γ) of the power-law radiation in the Compton cloud is (Sunyaev and Titarchuk, 1980);

$$\Gamma = \alpha + 1, \alpha = (9/4 + \gamma)^{1/2} - \frac{3}{2}$$
$$\gamma = \frac{\pi^2 m_e c^2}{3(\tau_o + 2/3)^2 kT_e} \tag{1}$$

Given this, the Titarchuk (1994) comptonization model was added in "*M3*" (*PL+diskbb+grad+gaus+CompTT;* M4) to constrain the plasma temperature (kT_e) and optical depth (τ_o; must be less than one for the optically thin plasma). The "*M4*" gives a good statistical fit with a reduced Chi-squared value of 1.0, and the F-test value/probability after adding *CompTT* is $4.84686/7.768 \times 10^{-09}$. The photon index was estimated empirically using Eq. (1), and the correlation of these parameters (kT_e, τ_o, Γ) gives a constant photon index value of 2.0. However, the *PL*–fitted photon index shows variations/fluctuations when correlated with the duo parameters (kT_e, τ_o) of *compTT*.

Moreover, while fitting these models (*M1, M2, M3 & M4*), the *grad* and *diskbb* models'–fitted parameters were consistently monitored to ensure their values were the same and/or comparable in the sequence of the fitting. This was achieved by using "steppar", and "newpar" techniques on the angle of inclination, optically thick mass accretion rate, mass of the source, etc. Thereafter, their average value of the parameters of *grad* and *diskbb* models were obtained and utilized in physical equations. The apparent radius, (r_i), of the accretion disk/flow, was estimated from the *diskbb* model's–fitted average normalization parameter; $\left(avgN_b = r_i^2 \cos\theta / D_{10}^2\right)$. The true radius, $R_i = \xi . K^2 . r_i$, of the accretion disk/flow (optically thick plasma) where the soft photons emitted was obtained. This was achieved by multiplying the apparent radius (r_i) with a correction factor (ξ= 0.50) and the squared spectral hardening factor (K^2 = 2.89; Shimura and Takahara, 1995; Kubota et al., 1998). Also, the average value of the accretion disk/flow mass accretion rate ($\dot{M}_{disk}$) with inclination ($\theta = 60°$), mass (10 $M_\odot$), and distance (D; 6.5 kpc) of MAXI J1535–571, and hardening spectral factor were obtained from the *grad* model. These model's–fitted parameters were substituted into Eq. (2) to estimate the X-ray luminosity of the optically thick plasma (Kubota et al., 1998);

$$L_{op-thick} = \frac{3GM_\odot \dot{M}}{2R_i} \times \left(1 - \sqrt{\xi . K^2}\right) \tag{2}$$

The optically thick plasma radiate with semi-isotropic or anisotropic intensity and its X-ray flux ($F_{op\text{-}thick}$) was estimated using Eq. (3); Gierlinski et al., 1999);

$$F_{op-thick} = \left(\frac{L_{op-thick}}{2\pi D^2}\right)\cos\theta \tag{3}$$

The optically thin plasma/flow (corona/Compton cloud) emits non-thermal (power-law) radiations isotropically and its X-ray flux ($F_{op\text{-}thin}$) and luminosity ($L_{op\text{-}thin}$) were estimated using Eqs. (4) and (5); Makishima et al., 1986; Gierlinski et al., 1999);

$$F_{op-thick} + F_{op-thin} 2\cos\theta = 0.0165 * [N_b]\left(\frac{T_i}{1keV}\right)^3 \times photonss^{-1}cm^{-2} \tag{4}$$

$$L_{op-thin} = 4\pi D^2 F_{op-thin} \tag{5}$$

where T_i and N_b is the inner disk temperature and normalization parameter of *diskbb* model respectively. The mass accretion rate of the optically thin plasma/ flow was estimated using equation (6; Shidatsu et al., 2014);

$$\dot{M}_{op-thin} = \frac{L_{op-thin}}{\eta c^2} \tag{6}$$

where "η" and "c" is the radiative inefficiency (0.8) flow and velocity of light respectively.

The optically thick plasma/flow ($\dot{M}_{op\text{-}thick}$) and optically thin plasma/flow ($\dot{M}_{op\text{-}thin}$) mass accretion rates were scaled to Eddington mass accretion rate (M_{Edd}) using Eq. (7), and their correlation was obtained (see Fig. 4).

$$\dot{M}_{Edd} = \frac{L_{Edd}}{c^2} = \frac{4\pi GMm_p}{\sigma_T c} = 1.7422 \times 10^{16} kgs^{-1} \tag{7}$$

Furthermore, to determine the correlation of the mass accretion rate of components of the accretion flow using another approach, the MAXI J1535–571 data was modelled with *TCAF* v0.3.2_R1 alongside *tbabs* (*tbabs***TCAF: M5;* Chakrabarti and Manickan, 2000; Debnath et al., 2014; Nandi et al., 2018) to constrain the Keplerian mass accretion rate (m_{dot}d) and sub-Keplerian mass accretion rates (m_{dot}h) in Eddington limit. This gives a reduced Chi-squared value of 1.38 (645.06/465) after the m_{dot}d and m_{dot}h were "steppar". Thereafter, a systematic error of 3% was used, and a reduced Chi-squared value of 1.11 (518.06/465). This gives a compression ratio (R) and shock strength (Xs) of 4.0 and 44.10 r_g respectively. A 2-D plot of m_{dot}d and m_{dot}h in logarithm scale was obtained (see Fig. 5a). Thereafter, m_{dot}d and m_{dot}h were linear "steppar" to run over fifty (30) grids/iterations to obtain a color-coded contour fit-statistic plot at different confidence levels (see Fig. 5b).

For temporal characteristics, QPOs are the most important among other temporal characteristics of the accretion flow, and resonance phenomenon is an indication of the presence of QPO in the hard spectral states (HS and HIMS; Chakrabarti, 2015), and the post-shock region must be in hydrostatic equilibrium (Chakrabarti and Manickam, 2000) to intercept the seed soft photons originating from the Keplerian region with X-ray flux (Chakrabarti and Titarchuk, 1995);

$$F_{ss} = 7.6 \times 10^{26} r^{-3} I \left(\frac{M}{M_\odot}\right)^2 \left(\frac{\dot{M}_d}{1.4 \times 10^{17}}\right) ergcm^{-2}S^{-1}$$
$$I = 1 - (3/r)^{1/2}, \dot{M}_d = m_{dotd} \times M_{Edd} \tag{8}$$

where $\dot{M}_d$, M, and "r" is the Keplerian mass accretion rate (in grams/s), the mass of the black hole (in solar mass), and inner radius at which the seed soft photon emits respectively.

The percentage of the intercepted seed soft photons by hot electrons is the shock height (H_s);

$$H_s = \left[\frac{\gamma(R-1)X_s^2}{R^2}\right]^{1/2} \tag{9}$$

The shock temperature is;

$$T_s = \frac{m_p(R-1)c^2}{2R^2 k_B (X_s - 1)} \tag{10}$$

where Xs, R, k_B, m_p, and γ in Eqs. (9) and (10) is the shock location/ strength, compression ratio, Boltzmann constant, mass of proton, and spherical adiabatic flow (5/3; polytropic index in the halo) respectively (Debnath et al., 2014). The shock height and temperature determine the degree of interception and inverse-comptonization of the seed soft photons. A compression ratio of 4 and shock strength of ≥ 38 r_g indicates that the oscillating shock is strong (Chakrabarti and Manickam, 2000), and the frequency of the oscillating shock (QPO) can be estimated empirically (Debnath et al., 2014);

$$\nu_{qpo} = \frac{c}{2\pi R r_g X_s (X_s - 1)^{1/2}} = \frac{\nu_{so}}{2\pi R X_s (X_s - 1)^{1/2}} \tag{11}$$

where $r_g = 2GM_{bh}/c^2$, G, c, and $\nu_{so} = c/r_g = c^3/2GM_{bh}$ is the radial distance (unit of Schwarzchild radius), the gravitational constant, speed of light, and inverse of light-travel time across the black hole of mass in s^{-1} respectively. The resonance phenomenon is feasible when the cooling (Keplerian flow) timescale (t_c) and infall (sub-Keplerian flow) timescale (t_i) are comparable ($t_c \sim t_i$; Molteni et al., 1995, 1996; Chakrabarti, 2015);

$$\tau_r = \frac{t_c}{t_i} = 3.5 \times 10^{-4} \left(\frac{1 + A_r}{f_o \lambda}\right)\left(1 - \frac{1}{R^2}\right) = 0.5 < \tau_r < 1.5 \tag{12}$$

where $A_r = \dot{M}_h + \dot{M}_d / \dot{M}_d$ is the ratio of the mass accretion flow rate (Keplerian + sub-Keplerian) to that of the Keplerian flow rate in kilograms/second. $\dot{M}_h = m_{doth} \times M_{Edd}$. "$f_o$" is the fraction of the intercepted seed soft photons that are comptonized in the post-shock region. "λ" is an average factor that determines the enhancement of the intercepted soft photon's energy in the post-shock region. "R" is the compression ratio that determines how the intercepted soft photons douse or slow comptonization by hot electrons. The values of "R", "λ", "f_o", and "A_r" in the hard states (HS and HIMS) vary in the range of 4 – 7, 10 – 40, 0.01 – 0.05, and 10^2 – 10^4 respectively. However, their respective value in the soft states (SIMS and SS) is 1, 1, 0, and 0 (Chakrabarti & Titarchuk, 1995; Chakrabarti and Manickam, 2000; Chakrabarti, Mondal, & Debnath, 2015; Chakrabarti, 2015). Given this, the spectral fitting was re-normalized and the *diskbb* model alongside power-law dense matter absorption (*PL)* and narrow Gaussian line (*Gaus*) was added one after the other to "*M5*". The aim was to constrain the model's–fit parameters to be utilized in the physical equations (8 – 12) to determine the X-ray flux of the soft photons reaching the post-shock/Compton cloud, shock height and temperature, frequency of QPO, the resonance condition, the timescales of components of the accretion flow, and the Γ–νQPO relation, as well as their correlation with the $m_{dot}d$ and $m_{dot}h$. The fit-statistic improved with a reduced Chi-squared value of 1.311 (607.21/463) and F-test value/probability of 14.4304/ 8.327 × 10^{-7} when the *diskbb* model was added. Also, adding the *PL* model improved the fit-statistic with a reduced Chi-squared value of 1.29(595.05/460), but when the cut-off energy and e-fold energy of the electron were "thawed" and the hydrogen column density of the *PL* model was frozen, the fit statistic significantly improved with a reduced Chi-squared value of 1.072(491.05/458) and F-test value/probability of 48.5002/7.853 × 10^{-20}. Adding the 6.5 keV *Gaussian* line improved the fit-statistic with a reduced Chi-squared value of 0.84 (382.39/455) and F-test value/probability of 43.0976/1.57244 × 10^{-24}. Hence, the composite model [*tbabs*(TCAF+diskbb +PL+gaus)*] is hereby referred to as "*M6*". The best-fit power-law photon index, compression ratio, and shock strength of 2.29, 3.99, and 44.91 r_g were obtained respectively. Therefore, the power-law photon index of (Γ; 2.0 – 2.3) from the aforementioned models affirms that MAXI J1535-571 is in the HIMS (Tao et al., 2018; Nakahira et al., 2018). Also, the compression ratio of 3.99 – 4 and shock strength of ≥ 38 r_g indicates that there is a strong quasi-periodic oscillating shock (Chakrabarti and Manickam, 2000) in the accretion flow. Given this, we used the *diskbb* model's normalization parameter of "*M6*" (alongside θ = 60°, M = 10 $M_\odot$, and D = 6.5 kpc constrained from the *grad* model) to estimate the apparent radius of the inner regions of the Keplerian flow (optically thick plasma) where the soft photons originate. Thereafter, the apparent radius was multiplied with correction and spectral hardening factors to obtain the true radius (Kubota et al., 1998). The Keplerian mass accretion rate ($M_{dot}d = m_{dot}d \times M_{Edd}$, in kilograms/second) obtained from the *TCAF* model alongside the true radius obtained from the *diskbb* was substituted into equation (8) to estimate the X-ray flux (Fss) of the soft photons. The post-shock height (Hs) and temperature(Ts) were estimated using the *TCAF* model's–fitted parameters in equations (9) and (10) respectively. Hence, the correlation of these three (Fss, Hs, Ts) parameters was obtained. The frequency of quasi-periodic oscillating shock was estimated using equation (11), and the Γ–νQPO correlation was obtained (see Fig. 6). We also obtained the correlation of the photon index with the $m_{dot}d$ and $m_{dot}h$ (see Fig. 7b, & c.). Moreover, we adopted 0.03 and 20 for "f_o" and "λ" respectively and substituted them alongside the values of A_r and R into equation (12) to estimate the resonance condition. The sub-Keplerian (infall) timescale was estimated using equation (13; Depnath, Chakrabarti, and Mondal, 2014);

$$t_i = X_s \big/ V_+ \sim RX_s(X_s - 1)^{1/2} \tag{13}$$

where $V_+ = 1/(X_s - 1)^{1/2}$is the velocity of the propagating waves in the post-shock region.

Thereafter, the values of the infall timescale were substituted into Eq. (12) to estimate the cooling timescale, and their correlation was obtained (see Fig. 10).

Furthermore, to checkmate the consistency of different models reproducing the accretion flow characteristics of the MAXI J1535–571. We re-normalized and fitted/modelled the data again by replacing the power-law dense matter absorption (*PL)* model in "*M6*" with the *nthcomp* model. Hence, [*tbabs*(TCAF+diskbb+nthcomp+gaus; M7)*]. This was done to check if we can obtain Γ–νQPO relation and other accretion flow characteristics consistent with that obtained in "*M6*". The significance of adding the *diskbb* to the *tbabs*(TCAF)* model has been given in "*M6*" and the *nthcomp* model was added. The seed photon temperature of the *nthcomp* model was "thawed" and tied to the temperature of the accretion disk of the *diskbb* model such that both parameters have the same value and represent the thermal temperature component of the accretion flow. This gives a reduced Chi-squared value of 1.36 (627.64/459) with an F-test/probability value of 35.6295/ 6.19141 × 10^{-26}. Thereafter, the *gaus* model was added and the statistical fit was improved with a reduced Chi-squared value of 1.16 (531.16/456) with an F-test/probability value of 27.6093/ 2.01368 × 10^{-16} and best-fit photon index of 2.11. The codes of all the physical equations and plotting of variables were done using MATLAB v8.3, and some irrelevant data points from the desired plot were removed using a*xes commands.* The standard errors in models'–fitted parameters utilized in physical equations was estimated using MATLAB. Also, Pearson product-moment correlation was used to determine the correlation coefficient (R) between plotted parameters on the vertical axis against the one on the horizontal axis (see Fig. 2 to Fig. 10; Fig. 5b was excluded) with p-values, lower (RL) and upper (RU) bounds for 95 % confidence interval. This was done using MATLAB syntax [*R, P, RL, RU*] = *corrcoef (…)* which returns a 2 × 2 matrix each for R, P, RL, and RU respectively, and their off-diagonal value were used to represent them (see Table 3).

3.2. Results

In comparison to other models, the "*M2*" and "*M6*" are the best models that prescribed the MAXI J1535–571 data very well based on the F-statistics test. Table 2 shows the F-test value of additive models and their significant contribution in fitting the data. The larger the F-test value, the lower the probability; hence, significant improvement in statistical fit due to the additional component model. The probability decreases as the F-test value increases. We chose to report the best-fit parameters of "*M6*", because it comprises the phenomenological and the physical models, though when the *Gaussian line* was added, the F-test value decreased a bit. Table 1 shows the best-fit spectral parameters of "*M6*". Table 3 shows the Pearson product-moment correlation of the parameters.

In Tables 1; N_H is the hydrogen absorption column density *mdotd_TCAF, mdoth_TCAF, M_TCAF, Xs_TCAF, R_TCAF, norm_TCAF,* is the Keplerian mass accretion rate, sub-Keplerian mass accretion rate, mass of the black hole, shock location (unit in gravitational radius), compression ratio, and normalization parameter of TCAF model respectively. Ti_diskbb and norm_diskbb are the inner temperature and normalization parameters of the multi-color component radiation respectively. Γ_PL, highecut_PL, E-fold_PL, and norm_PL are the power-law photo-index, high cut-off threshold, and e-folding energy and normalization factor of dense matter absorption power-law model respectively. E6.5_gaus, sigma_gaus, and norm_gaus is the line energy, line width and normalization parameter of the 6.5 keV narrow Gaussian emission model respectively. d.o.f is the degree of freedom.

The errors in each spectral parameter in Table 1 were determined

Table 1
shows the best-fit spectral parameters of "M6".

Best-fit parameters/units	Values ± error
N_H (cm^{-2})	4.213×10^{22}
$m_{dot}d$_TCAF (M_{Edd})	$0.254^{0.059}_{-0.157}$
$m_{dot}h$_TCAF (M_{Edd})	$0.119^{0.066}_{-0.016}$
M_TCAF ($M_\odot$)	10.027 ± 0.01
Xs_TCAF (r_g)	44.801 ± 0.20
R_TCAF	4.000 ± 0.12
norm_TCAF	$70.81^{0.14}_{-0.02}$
Ti_diskbb (keV)	$0.644^{0.305}_{-0.115}$
norm_diskbb	$159.214^{1.390}_{-0.384}$
Γ_PL	2.29 ± 0.21
highecut_PL (keV)	24.637 ± 0.573
E-fold_PL (keV)	27.912 ± 0.616
norm_PL	$11.074^{1.761}_{-0.507}$
$E_{6.5}$_gaus (keV)	$6.53^{0.04}_{-0.02}$
sigma_gaus (keV)	$2.032^{0.529}_{-0.319}$
norm_gaus	$0.638^{0.339}_{-0.209}$
Chi-squared	382.39
d.o.f	455
Reduced chi-squared	0.84
Null hypothesis	9.942×10^{-01}

Table 2
F-test value of the additive component models and their significance.

Model 1 (M1)	tbabs*(bmc*highecut+diskbb)	tbabs*(bmc*highecut+diskbb+bbody)	tbabs*(bmc*highecut+diskbb+bbody+grad)	tbabs*(bmc*highecut+diskbb+bbody+grad+gaus)	—
Chi-squared	2960.91	608.71	549.89	533.37	—
d.o.f	463	461	456	455	—
Reduced chi-squared	6.39505	1.3204	1.2059	1.1722	—
F-test value/ probability	—	890.707/ 4.39638e-159	9.75538/ 7.21304e-09	14.0927/ 1.96568e-09	—
Model 2 (M2)	tbabs*(nthcomp+diskbb)	tbabs*(nthcomp+diskbb+grad)	babs*(nthcomp+diskbb+grad+gaus)	—	—
Chi-squared	682.17	641.02	531.38		—
d.o.f	465	460	457		—
Reduced chi-squared	1.4670	1.3935	1.1628	—	—
F-test value/ probability	—	5.91164/ 2.60738e-05	31.431/ 1.73224e-18	—	—
Model 3 (M3)	(PL+diskbb)	(PL+diskbb+grad)	(PL+diskbb+grad+gaus)	—	—
Chi-squared	736.06	534.10	515.09		—
d.o.f	465	460	457		—
Reduced chi-squared	1.5829	1.1611	1.1271	—	—
F-test value/ probability	—	34.7881/3.55307e-30	5.62204/0.000861995	—	—
Model 4 (M4)	—	—	—	(PL+diskbb+grad+gausCompTT)	—
Chi-squared	—	—	—	493.95	—
d.o.f				453	—
Reduced chi-squared	—	—	—	1.0904	—
F-test value/ probability	—	—	—	4.84686/0.000776844	—
Model 5 (M5)	tbabs*(TCAF)	—	—	—	—
Chi-squared	645.06	—	—	—	—
d.o.f	465	—	—	—	—
Reduced chi-squared	1.3872	—	—	—	—
F-test value/ probability	—	—	—	—	—
Model 6 (M6)	tbabs*(TCAF)	tbabs*(TCAF+diskbb)	tbabs*(TCAF+diskbb+PL)	tbabs*(TCAF+diskbb+PL)Ecut and e-fold thawed and N_H freezed	tbabs*(TCAF+diskbb+PL+gaus)
Chi-squared	645.06	607.21	595.05	491.05	382.39
d.o.f	465	463	460	458	455
Reduced chi-squared	1.3872	1.3115	1.2936	1.0722	0.84041
F-test value/ probability	—	14.4304/ 8.32785e-07	31.3341/ 0.0253768	48.5002/7.8532e-20	43.0976/ 1.57244e-24
Model 7 (M7)	tbabs*(TCAF)	tbabs*(TCAF+diskbb)	tbabs*(TCAF+diskbb+nthcomp)	tbabs*(TCAF+diskbb+nthcomp+gaus)	—
Chi-squared	926.64	822.52	627.64	531.16	—
d.o.f	465	463	459	456	
Reduced chi-squared	1.9928	1.7765	1.3674	1.1648	—
F-test value/ probability	—	29.3048/ 1.03872e-12	35.6295/ 6.19141e-26	27.6093/ 2.01368e-16	—

Table 3
Pearson product-moment correlation of parameters.

Figures	parameter	Correlation coefficient (r)	P-value	Lower bound	Upper bound	Direction and strength of correlation	Is the test statistically significant?
Fig. 2	Γ vs $Norm_{bmc}$	0.8607	<0.0001	0.7715	0.9167	Very strong positive	yes
Fig. 3a	tau vs $Te_{\_CompTT}$	0.9988	<0.0001	0.9978	0.9993	Very strong positive	yes
	Γ vs $Te_{\_CompTT}$	0.00	1.00	−0.2872	0.272	No relation	no
Fig. 3b	tau vs $Te_{\_CompTT\ \&\ PL}$	0.9988	<0.0001	0.9978	0.9993	Very strong positive	yes
	$\Gamma_{\_PL}$ vs $Te_{\_CompTT}$	−0.9044	<0.0001	−0.9459	−0.8337	Very strong negative (anti-correlated)	yes
Fig. 4	M_{dot} d vs M_{dot} h	0.8415	<0.0001	0.7574	0.8981	Very strong positive	yes
Fig. 5a	m_{dot} d vs m_{dot} h _M5	−0.8373	<0.0001	−0.8871	−0.7682	Very strong negative (anti-correlation)	yes
Fig. 6a	Γ vs vQPO_M6	0.7694	<0.0001	0.6702	0.8416	Strong positive	yes
Fig. 6b	Γ vs vQPO_M7	0.2430	0.0383	0.0137	0.4480	Weak positive	yes
Fig. 7a	vQPO vs m_{dot} d	0.7866	<0.0001	0.6910	0.8551	Strong positive	yes
	m_{dot} h vs m_{dot} d	−0.8453	<0.0001	−0.8961	−0.7726	Very strong negative (anti-correlation)	yes
Fig. 7b	m_{dot} d vs Γ _M6	0.8530	<0.0001	0.7854	0.9005	Very strong positive	Yes
	m_{dot} h vs Γ_M6	−0.6386	<0.0001	−0.7459	−0.4991	Vtrong negative	yes
Fig. 7c	m_{dot} d vs Γ _M7	0.3972	0.0005	0.1840	0.5748	Weak positive	yes
	m_{dot} h vs Γ_M7	−0.5334	<0.0001	−0.6800	−0.3457	Moderate negative	yes
Fig. 8a	m_{dot} d vs (m_{dot} $(d+h)$)	0.9976	<0.0001	0.9963	0.9984	Very strong positive	yes
	m_{dot} h vs (m_{dot} $(d+h)$)	−0.8059	<0.0001	−0.8687	−0.7176	Very strong negative	yes
Fig. 8b	Fss vs (m_{dot} $(d+h)$)	0.6908	<0.0001	0.5628	0.7864	Strong positive	yes
	Γ vs (m_{dot} $(d+h)$)	0.9810	<0.0001	0.9710	0.9875	Very strong positive	yes
Fig. 8c	m_{dot} d vs Fss	0.6494	<0.0001	0.5092	0.7560	Strong positive	yes
	m_{dot} h vs Fss	−0.2198	0.0396	−0.4104	−0.0109	Weak negative	yes
Fig. 9	Ts vs Fss	0.4553	<0.0001	0.2718	0.6069	Moderate positive	yes
	Hs vs Fss	−0.4805	<0.0001	−0.6269	−0.3014	Moderate negative	yes
Fig. 10	t_c vs (m_{dot} $(d+h)$)	−0.9471	<0.0001	−0.9584	−0.9054	Very strong negative	yes
	t_i vs (m_{dot} $(d+h)$)	−0.8641	<0.0001	−0.9091	−0.7994	Very strong negative	yes

The parameter is the photon index (Γ), normalization parameter of the bmc model ($Norm_{bmc}$), optical depth (tau), electron temperature (Te), optically thick flow/plasma mass accretion rate(M_{dot}d), optically thin flow/plasma mass accretion rate,(M_{dot}h), Keplerian flow mass accretion rate (m_{dot}d), sub-Keplerian flow mass accretion rate (m_{dot}h), frequency of quasi-periodic oscillation (vQPO), accretion flow rate [($m_{dot}$$(d+h)$)], X-ray flux of intercepted soft photons (Fss), shock temperature (Ts), shock height (Hs), cooling time scale (t_c), infall timescale (t_i) respectively. The p-value <0.0001 indicates that the actual value p-value is too small for the MATLAB software to display, but the relation between the parameters is statistically significant.

using *XSPEC error* command at a 95 % confidence range. We deem it unnecessary to present the X-ray spectrum of MAXI J1535–571 obtained from each model. Fig. 1a, b, and c is the X-ray spectrum of MAXI J1535–571 obtained using phenomenological models, physical (*TCAF*) model, and "M6" respectively. These models give a good and robust statistically acceptable fit. The models consistently reproduced the power-law best-fit photon index in the range of 2.0–2.29. Fig. 2 is the correlation of the power-law photon index and normalization parameter (of the *bmc* model). The photon index increases from 1.517 to 1.542 as $Norm_{bmc}$ parameter increases from 0.3223 to 0.3384, but later attained saturation at 1.666–1.67 with further increase in $Norm_{bmc}$ parameter. This suggests that the photon index increases with the increase in the optically thick flow mass accretion rate. The correlation between the photon index and the normalization parameter is strong and statistically significant with a correlation coefficient of 0.86. Fig. 3a is the correlation of photon index and plasma temperature and optical depth in the Compton cloud using Titarchuk's (1994) comptonization model's–fitted parameters. The photon index is relatively constant with a value of 2.02 while the temperature and optical depth increase in unison. The photon index estimated from *CompTT* and electron temperature have zero coefficients. Hence, there is no association between them. However, the correlation of *CompTT* (kT_e, τ_o) parameters with the photon index of the *PL* model as shown in Fig. 3b reveals that the photon index varies and fluctuates with an increase in temperature and optical depth. Fig. 4 shows the variations of the optically thick flow mass accretion rate ($\dot{M}_{op\text{-}thick}$) and optically thin flow mass accretion rate ($\dot{M}_{op\text{-}thin}$) in the Eddington limit obtained using models'–fitted averaged parameters of the *diskbb* and *grad* models and physical equations. Both the $\dot{M}_{op\text{-}thick}$ and $\dot{M}_{op\text{-}thin}$ are linearly correlated with a coefficient of 0.84, but there is an indication of fluctuation in $\dot{M}_{op\text{-}thin}$ between 0.0505 M_{Edd} and 0.04142 M_{Edd}. Fig. 5a shows the Keplerian flow mass accretion rate (m_{dot}d) and sub-Keplerian flow mass accretion rate (m_{dot}h) are anti-correlated. As m_{dot}h decreases from 0.007423 M_{Edd} to 0.004359 M_{edd} while m_{dot}d is relatively constant (0.001025 M_{Edd}). Thereafter, m_{dot}h is relatively constant for further increase in m_{dot}d. This indicates the independent variations of m_{dot}d and m_{dot}h. Fig. 5b shows the fit statistics color-contour plot of m_{dot}d and m_{dot}h obtained from "*M5*". This portrays the elaborate variations of m_{dot}d and m_{dot}h at three different confidence intervals. The plus sign "+" (8.312×10^2) corresponds to the minimum fit statistic. The middle and upper fit statistic level is 8.335×10^2 and 8.404×10^2 respectively. The color bar on the right hand is the delta-fit statistic.

Fig. 6 shows the positive correlation between the power-law photon index and the frequency of the QPO (Γ–vQPO). Fig. 6a and 6b were obtained using "*M 6″* and "*M7*" fitted data respectively. The photon index increases linearly with the frequency of QPO but saturates with a further increase in frequency. The Γ–vQPO relation of "M6" has a strong correlation while that of the "M7" is weak with coefficients of 0.76 and 0.24 respectively. Also, there are indications of fluctuation in both values of photon index (between 1.915 to 1.928; Fig. 6b) and frequency of QPO (between 1.574 Hz to 1.656 Hz; Fig. 6a). The fluctuation and saturation effect is believed to be associated with the intrinsic characteristics of the accretion flow; mass accretion rates. Fig. 7a shows the correlation of frequency of QPO and m_{dot}h versus m_{dot}d. An increase in m_{dot}d leads to an increase in the frequency of QPO (vQPO) and a decrease in m_{dot}h. Also, m_{dot}d, vQPO, and m_{dot}h saturate and fluctuate at some points. The m_{dot}d and vQPO are positively correlated with a coefficient of 0.78 whereas m_{dot}d and m_{dot}h are anti-correlated with a coefficient of –0.84. This suggests that variations/fluctuations as well as saturation effect in m_{dot}d and m_{dot}h have a strong impact on the vQPO.

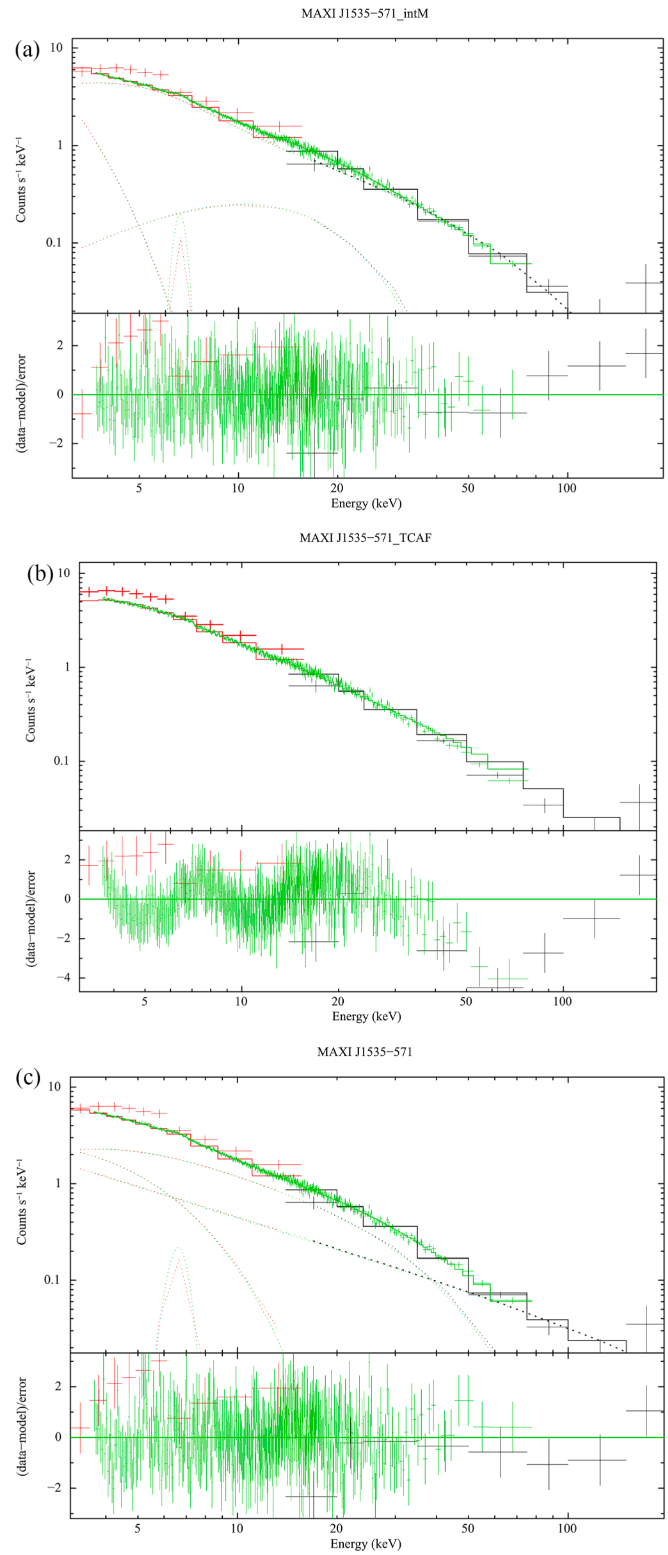

(caption on next column)

Fig. 1. (**a**) X-ray spectrum of MAXI*J1535–571* obtained phenomenological models "M2". In the upper panel, the fitted data are shown by crosses; *NuSTAR* data is green, MAXI/GSC data is red, and *Swift/BAT data is black, whereas the* XSPEC models are represented by the solid thick, and broken lines. The peak of the broken green and red curve shows the Gaussian of the iron emission line at 6.5 keV. The lower panel shows the ratio of the fitted data to the models.; (**b**) X-ray spectrum of MAXIJ1535–571 obtained using physical (*TCAF*) model. In the upper panel, the fitted data are shown by crosses; *NuSTAR* data is green, *MAXI/GSC* data is red, and *Swift/BAT* data is black, whereas the *TCAF* model ("*M5*") is represented by the solid thick line. The lower panel shows the ratio of the fitted data to the models.; **(c)** X-ray spectrum of MAXI J1535–571 obtained using phenomenological and physical models ("*M6*"). In the upper panel, the fitted data are shown by crosses; *NuSTAR* data is green, *MAXI/GSC* data is red, and *Swift/BAT* data is black, whereas the phenomenological and physical models are represented by the solid thick, and broken lines. The peak of the broken green and red curve shows the Gaussian of the iron emission line at 6.5 keV. The lower panel shows the ratio of the fitted data to the models.

Fig. 7b&c shows the variations/fluctuations of $m_{dot}d$ and $m_{dot}h$ with photon index. Abinitio, $m_{dot}d$, and $m_{dot}h$ increase while the photon index decreases. Thereafter, the photon index increases and saturates at some points with an increase in $m_{dot}d$ while the $m_{dot}h$ decreases. Later, both $m_{dot}d$ and $m_{dot}h$ fluctuate and saturate as the photon index increases. The $m_{dot}d$ and photon index are linearly correlated while $m_{dot}h$ is anti-correlated with the photon index (see Table 3). This suggests that the independent variations/fluctuations of $m_{dot}d$ and $m_{dot}h$ can determine the variations/fluctuations and saturation effect in the photon index.

Fig. 8a is the correlation of $m_{dot}d$ and $m_{dot}h$ and mass accretion flow rate [$m_{dot}(d+h)$]; sum of Keplerian and sub-Keplerian mass accretion rates] in the Eddington limit. Both $m_{dot}d$ and $m_{dot}(d+h)$ increase linearly with each other while $m_{dot}h$ is anti-correlated with them at first instance, but later, $m_{dot}h$ increases in unison with $m_{dot}d$ and $m_{dot}(d+h)$. Thereafter, $m_{dot}d$ exhibited little reverse track from 0.2383 M_{Edd} to 0.2372 M_{Edd} that resulted in a "kink" or curve shape in $m_{dot}h$ track and a decrease in $m_{dot}(d+h)$ from 0.3224 M_{Edd} to 0.321 M_{Edd}. That is, a drop in the value of $m_{dot}d$ causes a corresponding drop in the values of $m_{dot}(d+h)$ and $m_{dot}h$ (0.088421 M_{Edd} to 0.0838 M_{Edd}). Later, $m_{dot}h$ increases in unison with $m_{dot}d$ and $m_{dot}(d+h)$. $m_{dot}d$ is positively correlated with $m_{dot}(d+h)$ while $m_{dot}h$ is anti-correlated with $m_{dot}(d+h)$. This indicates that the variations/fluctuations in $m_{dot}h$ and $m_{dot}(d+h)$ are regulated by the variations/fluctuations in $m_{dot}d$. In other words, the dramatic changes in the values of $m_{dot}h$, and $m_{dot}(d+h)$ suggest intermittent/flickering behavior believed to be mastermind by the $m_{dot}d$. Fig. 8b shows the positive correlation of X-ray flux of the intercepted soft photons (Fss) and photon index (Γ) versus accretion flow rate [$m_{dot}(d+h)$]. Both the X-ray flux of soft photon (1.542×10^{-9} erg cm^{-2}s^{-1} to 7.168×10^{-8} erg cm^{-2}s^{-1}) and the photon index (1.713 to 1.859) increases in unison with an increase in $m_{dot}(d+h)$. However, a drop in $m_{dot}(d+h)$ from 0.3224 M_{Edd} to 0.3209 M_{Edd} created a corresponding effect in Fss and Γ respectively. This is an indication of fluctuation believed to be regulated by the variations/fluctuations in $m_{dot}d$ and $m_{dot}h$ since $m_{dot}(d+h)$ solely depends on them. Moreover, the increase in photon index in unison with Fss suggests that the gradual interception and comptonization of Keplerian flow in the post-shock region (Compton cloud/corona) leads to cooling and softening of the hard X-ray spectrum. Fig. 8c shows the correlation of the X-ray flux of the intercepted soft photon (Fss) and $m_{dot}d$ and $m_{dot}h$. The $m_{dot}d$ and $m_{dot}h$ are anti-correlated, fluctuate, and positively correlated to each other in unison with an increase in Fss. The respective variations in the values of $m_{dot}d$ and $m_{dot}h$ are not significant when they are positively correlated. This indicates saturation. The $m_{dot}d$ and Fss are positively correlated while $m_{dot}h$ is anti-correlated with the Fss. This suggests that the probable cause of variations/fluctuations and saturation effect in Fss and other accretion flow characteristics are $m_{dot}d$ and $m_{dot}h$. Fig. 9 shows the correlation of post-shock temperature (Ts) and post-shock

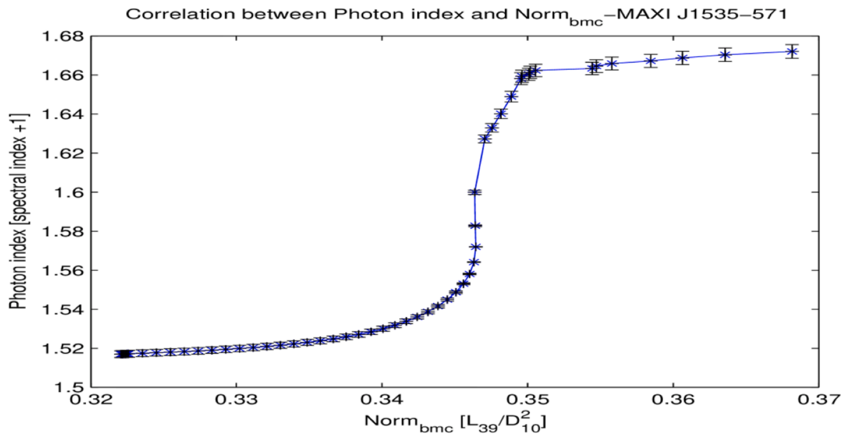

Fig. 2. Correlation of Photon index and Norm$_{bmc}$ parameter obtained using the *bmc* model parameters ("*M1*"). The data is asterisk (*; blue) whereas the error associated with each data point is the solid black cross with cap.

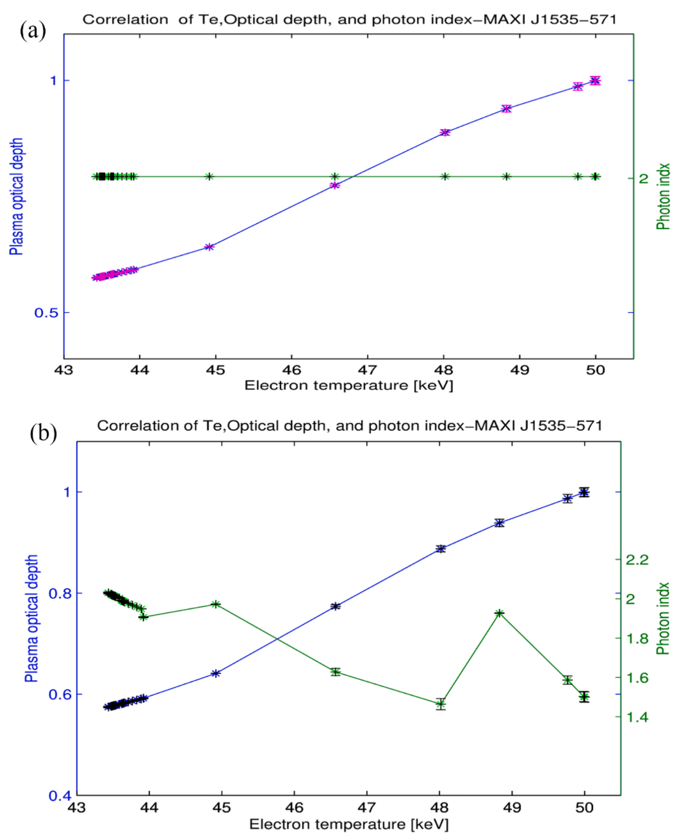

Fig. 3. **(a)** Correlation of Optical depth, and Photon index vs Electron Temperature obtained using *CompTT* fitted parameters ("*M4*"). The data is asterisk (*; optical depth is magenta, Γ is green) whereas the error associated with each data point is the solid black cross.; **(b)** Correlation of Optical depth, and Photon index vs Electron Temperature obtained using the *PL* and *CompTT* model-fitted parameters ("*M4*"). The data is asterisk (*; tau is blue, Γ is green) whereas the error associated with each data point is the solid black cross with cap.

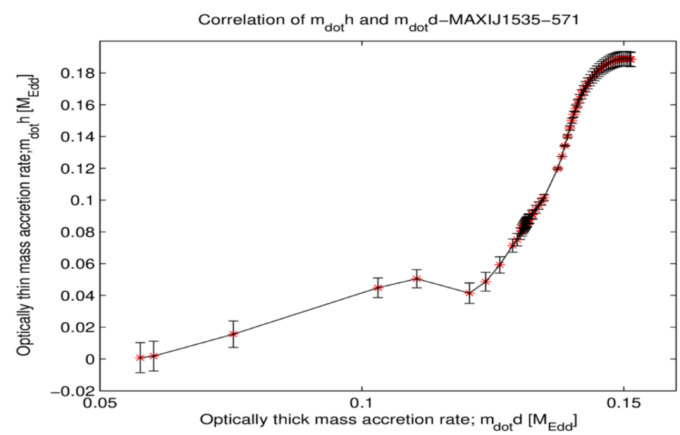

Fig. 4. Correlation of optically thin and optically thick flow mass accretion rates obtained using *diskbb* and *grad* models'–fitted parameters. The data is asterisk (*; red) whereas the error associated with each data point is the solid black cross with cap.

height (Hs). As Fss increases, Ts increases and attains its peak while Hs decreases and attains its valley. Thereafter, Ts gradually decreased while Hs gradually increased with a further increase in Fss. Hence, Ts and Hs are anti-correlated. The variations in both values of Hs (1.962×10^{11} m to 2.039×10^{11} m) and Ts (9.103×10^{5} K to 8.93×10^{5} K) were not significant when the Fss increased from 5.47×10^{-8} erg cm^{-2}s^{-1} to 7.136×10^{-8} erg cm^{-2}s^{-1}. This indicates that Hs and Ts tend to saturate. Fig. 10 shows the correlation of the infall timescale (t_i) and cooling timescale (t_c), and accretion flow rate. The infall and cooling timescales decrease with an increase in accretion flow rate till the accretion flow rate ($m_{dot}(d + h)$) is 0.3485. Thereafter, both the infall and cooling timescales increase in unison with a further increase in $m_{dot}(d + h)$. The infall and cooling timescales are roughly matched, and their strong anti-correlation with the $m_{dot}(d + h)$ are statistically significant (see Table 3).

4. Discussion and conclusion

We can deduce from the spectral results that MAXI J1535–571 accretion flow consists of two components; optically thin (sub-Keplerian) and optically thick (Keplerian) flow/plasma just like other transient BHBs/BHCs (Chakrabarti and Titarchuk, 1995; Gierlinaski et al., 1999; Kubota and Makishima, 2004; Banerjee et al., 2020). These components of the accretion flow coexist, and their dynamics are explained by the continuity, temperature, and pressure balance equations of the *XSPEC* and *TCAF*–models used (Chakrabarti, 1989; Chakrabarti and Titarchuk, 1995, 1997; Kubota et al., 1998; Borozdin et al., 1999; Laurent and Titarchuk, 1999; Kubota and Makishima, 2004; Debnath et al., 2014). The thermal–and inverse–comptonization of the seed soft photons by hot electrons in the Compton cloud/post-shock region of MAXI J1535–571 produce hard power-law X-rays in a similar way seen in other BHBs/BHCs during the hard states (Titarchuk, 1994; Esin et al., 1996; Zycki et al.,1999; Gierlinski et al., 1999; Gierlinski and Newton, 2006; Debnath et al., 2014). The best-fit power-law photon index

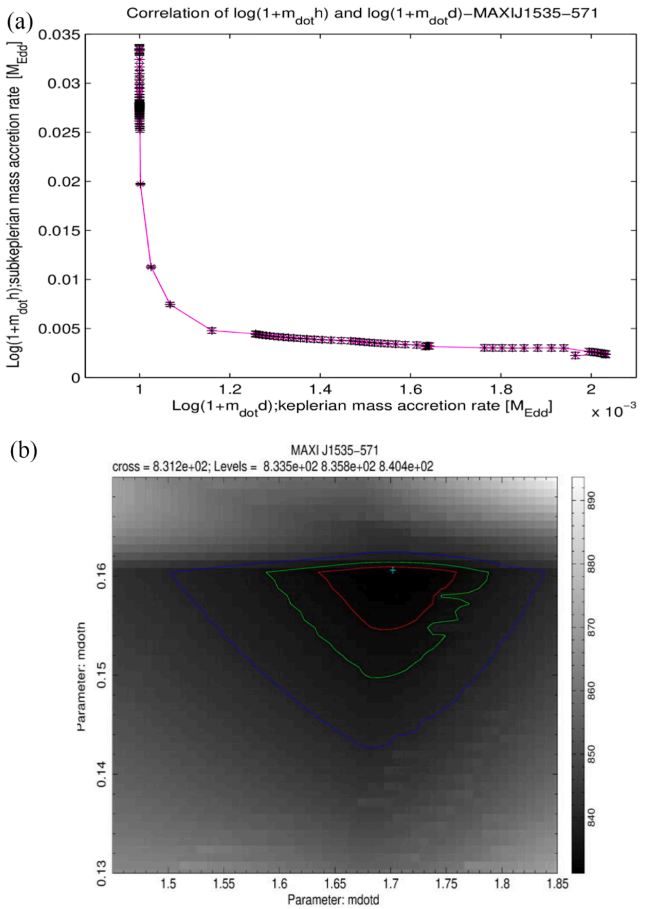

Fig. 5. (a) Correlation of sub-Keplerian flow and Keplerian flow mass accretion rates obtained using *TCAF* models'–fitted parameters. The data is asterisk (*; magenta) whereas the error associated with each data point is the solid black cross with cap.;**(b)** Contour plot of Keplerian flow and sub-Kepleria flow mass accretion rates at three different confidence levels obtained using *TCAF* models'–fitted parameters. The plus sign "+" represent the minimum fit statistic (8.312×10^2). The middle and upper fit statistic level is 8.335×10^2 and 8.404×10^2 respectively. The colorbar on the right hand is the delta-fit statistic.

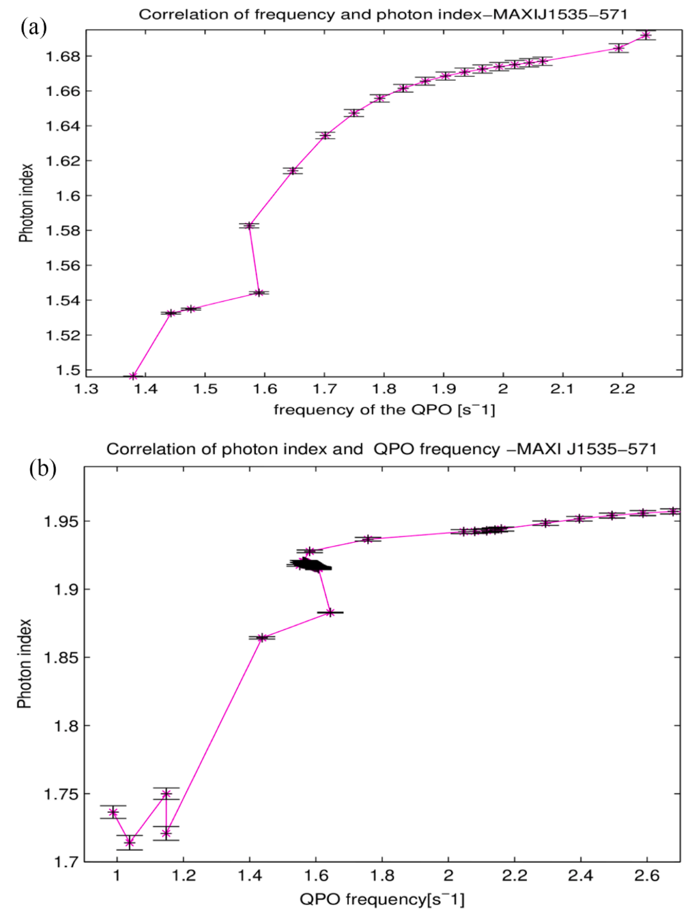

Fig. 6. (a) Correlation of Photon index and frequency of QPO obtained using "*M6*"– fitted parameters. The data is asterisk (*; magenta) whereas the error associated with each data point is the solid black cross with cap.; **(b)** Correlation of Photon index and frequency of QPO obtained using "*M7*"–fitted parameters. The data is asterisk (*; magenta) whereas the error associated with each data point is the solid black cross with cap.

obtained from our spectral analysis varies from 2.02 to 2.29 consistent with the photon index in the range of ∼ 1.8 to 2.3 observed in the HIMS of other galactic black hole sources (Esin et al., 1997; Esin et al., 1998; Remillard and McClintock, 2006). This affirms the hard-intermediate spectral states classification of MAXI J1535–571 (Tao et al., 2018; Nakahira et al., 2018). Also, we were able to obtain the track of Γ–Norm_{bmc} (see Fig. 2) which is an indication of converging flow and it is similar to what has been observed in other compact sources (Blandford and Payne,1981; Laurent and Titarchuk, 1999; Titarchuk et al., 2007, 2016; Titarchuk et al., 2020). Some accretion flow parameters/characteristics are linearly correlated while some are anti-correlated and their correlations are statistically significant, except the photon index plotted in Fig. 3a (see Table 3). A constant photon index of 2.02, while kT_e and τ_0 were varying indicates that the variations of spectral indices were not significant when fitted/modelled with the Titarchuk comptonization model (Titarchuk, 1994; Chakrabarti and Titarchuk, 1995). However, the photon index of the *PL* model varies, fluctuates, and saturates (see Fig. 3b) when correlated with the kT_e and τ_0 of *CompTT*. This is due to the power-law distribution of energy density regulated by variations/fluctuation in the components of accretion flow rates (Chakrabarti and Titarchuk, 1995; Yaqoob, 1997; Debnath et al., 2014). Our spectral analysis and results suggests that the components of the accretion flow in the HIMS coexist and interact with one another at varying distances as their mass accretion rates change (Chakrabarti and Titarchuk, 1995). Thus, the accretion flow is dynamic. The different adopted models used in this work reproduced the track of variations/-fluctuations of components of the accretion flow very well. The optically thin mass accretion rate ($\dot{M}_{\text{op-thin}}$) and optically thick ($\dot{M}_{\text{op-thick}}$) mass accretion rate increase in unison, but further increase in $\dot{M}_{\text{op-thick}}$ caused a drop and later saturation in $\dot{M}_{\text{op-thin}}$ (see Fig. 4). This indicates that variations in $\dot{M}_{\text{op-thick}}$ mediate the variations in $\dot{M}_{\text{op-thin}}$. Moreover, Keplerian mass accretion rate ($m_{dot}d$) is relatively constant when the sub-Keplerian mass accretion rate ($m_{dot}h$) is decreasing, but as $m_{dot}d$ increases, $m_{dot}h$ is relatively constant (see Fig. 5a). The contour plot shows a vivid variations/fluctuations in $m_{dot}d$ and $m_{dot}h$ in three different confidence intervals, and the "zig-zag" patterns indicates that $m_{dot}d$ and $m_{dot}h$ are strongly correlated (see Fig. 5b). The $m_{dot}d$ and $m_{dot}h$ are linearly correlated, anti-correlated, fluctuates and saturates at different phases (see Fig. 7b, c, & Fig. 8a). Also, our spectral analysis and results shows that the individual variations/fluctuations of optically thin (sub-Keplerian) and optically thick (Keplerian) flow/mass accretion rate variations (Ingram and Done, 2011) created propagating Quasi-periodic oscillation (QPO) in the accretion flow when their timescales roughly matched (see Fig. 10). The resonance condition (Molteni et al., 1995, 1996; Chakrabarti, 2015) in the range of 0.70 to 0.83 quantifies the presence of QPO with frequency in the range of 1.1 Hz to 2.7 Hz consistent with the results of Mereminskiy et al. (2018) and QPO frequency; 0.1 – 10 Hz, of Type-C (Casella et al., 2004; Motta et al., 2012). Therefore, the QPO in the accretion flow is likely Type-C which often

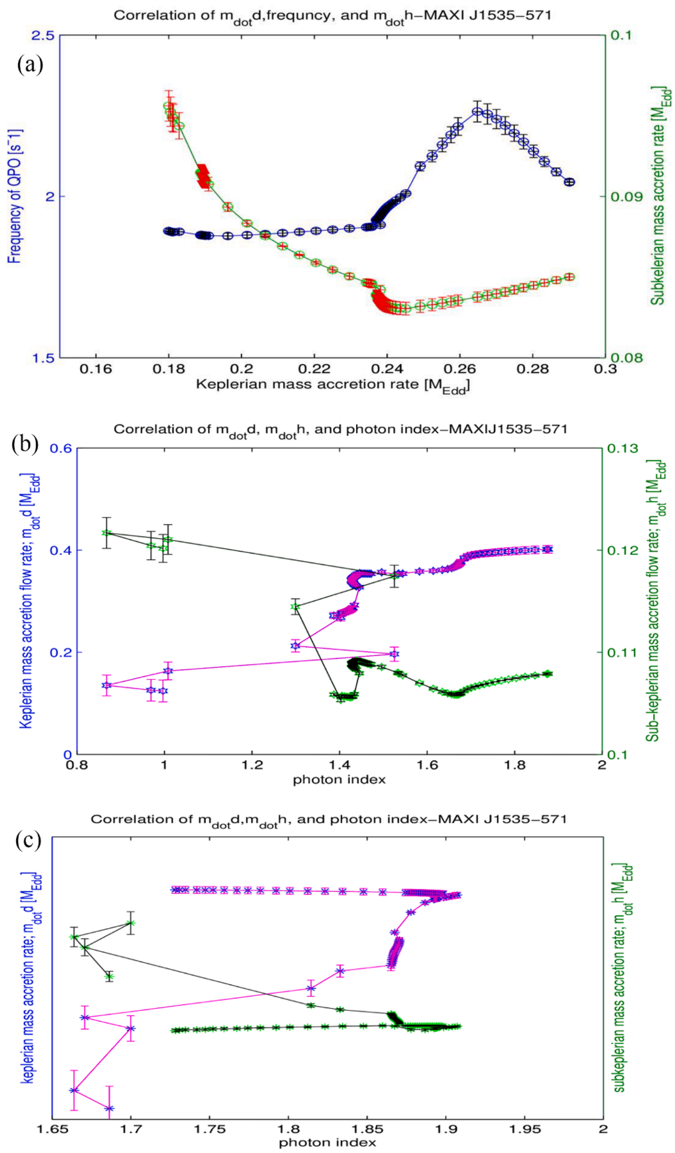

Fig. 7. **(a)** Correlation of Frequency of QPO, and m_{dot}h vs m_{dot}d obtained using "*M7*"–fitted parameters. The data is circle (frequency is blue, m_{dot}h is green) whereas the error associated with each data point is the solid black and red cross with cap respectively.; **(b)** Correlation of m_{dot}d and m_{dot}h vs Photon index obtained using "*M6*"–fitted parameters. The data is hexagram (m_{dot}d is blue, m_{dot}h is green) whereas the error associated with each data point is the solid magenta and black cross with cap respectively.; **(c)** Correlation of m_{dot}d and m_{dot}h vs Photon index obtained using "*M7*"– fitted parameters. The data is asterisk (*; m_{dot}d is blue, m_{dot}h is green) whereas the error associated with each data point is the solid magenta and black cross with cap respectively.

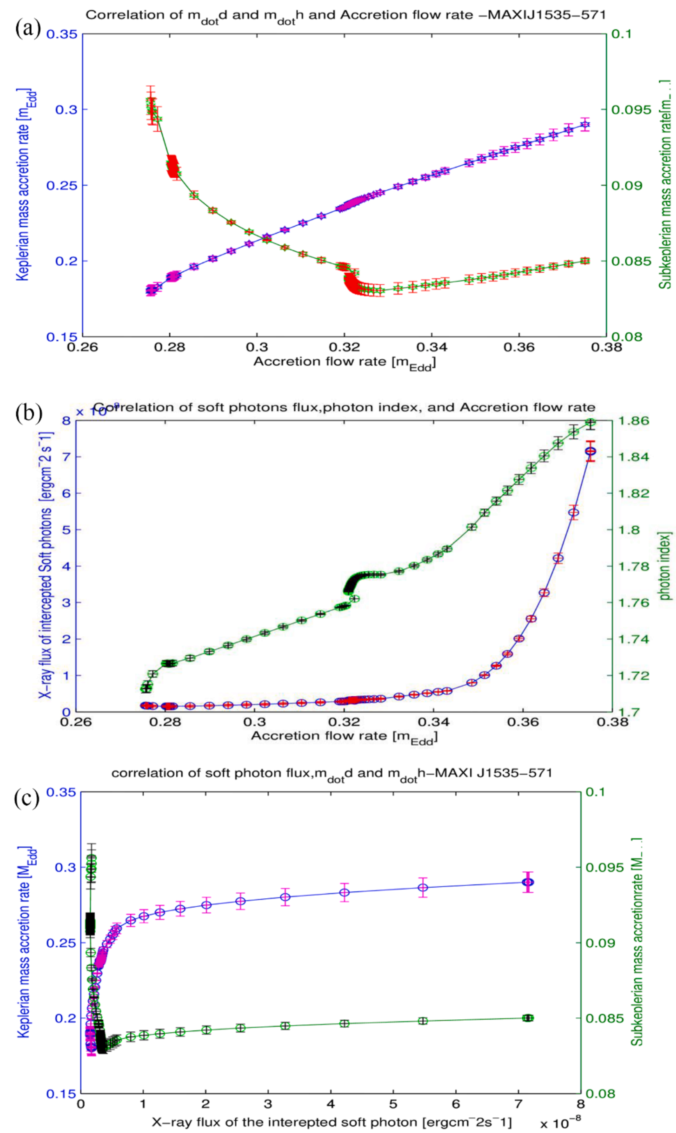

Fig. 8. **(a)** Correlation of m_{dot}d and m_{dot}h vs Accretion flow rate [m_{dot} $(d + h)$] obtained using "*M7*"–fitted parameters. The data is hexagram (m_{dot}d is blue, m_{dot}h is green) whereas the error associated with each data point is the solid magenta and red cross with cap respectively.; **(b)** Correlation of soft X-ray flux (Fss), photon index(Γ), vs Accretion flow rate (m_{dot} $(d + h)$) obtained using "*M7*"–fitted parameters. The data is circle (Fss is blue, Γ is green) whereas the error associated with each data point is the solid red and black cross with cap respectively.; **(c)** Correlation of m_{dot}d and m_{dot}h vs soft X-ray flux (Fss) obtained using "*M7*"– fitted parameter. The data is circle (m_{dot}d is blue, m_{dot}h is green) whereas the error associated with each data point is the solid magenta and black cross with cap respectively.

appears in the accretion flow during the HS and HIMS (Chakrabarti, 2015). The track of Γ–νQPO relation we obtained (see Fig. 6& Fig. 7) is positively correlated and statistically significant (see Table 3). This is similar to the Γ–νQPO track/relation obtained from the temporal analysis of MAXI J1535–571 and other BHCs (Molla et al., 2017; Mereminskiy et al., 2018; Stiele and Kong, 2018; Shang et al., 2019). The correlation of accretion flow characteristics with one another (see Fig. 7 to 9) indicates that m_{dot}d and m_{dot}h are intrinsic or hidden properties of the accretion flow in a variety of analytical, phenomenological, and physical accretion models (e.g. Laurent andTitarchuk, 1999; Done et al., 2007; Dunn et al., 2008; Molla et al., 2016, 2017; Debnath et al., 2017). The m_{dot}d and m_{dot}h are positively correlated, anti-correlated, fluctuate, and saturate at different phases and create corresponding physical phenomena in other accretion flow characteristics. Fig. 7 shows these corresponding physical properties on photon index and frequency of QPO. This suggests that Γ–νQPO track/relation and its origin are tied to the independent variations/fluctuations in the m_{dot}d and m_{dot}h. Moreover, variations/fluctuations in m_{dot}d and m_{dot}h create a corresponding effect in the accretion flow rate [$m_{dot}(d + h)$], soft photon X-ray flux (Fss), photon index, shock height (Hs) and shock temperature (Ts; see Fig. 8 and Fig. 9). A drop in the value of m_{dot}d and m_{dot}h creates a corresponding drop or reverse track in the accretion flow rate [$m_{dot}(d + h)$] and other accretion flow characteristics. The variations/fluctuations in m_{dot}d and m_{dot}h alter the height/size of the post-shock region, and the Hs and Ts are expected to decrease with an increase in the interception of soft photons, and suppression of coronal activities (Debnath et al.,

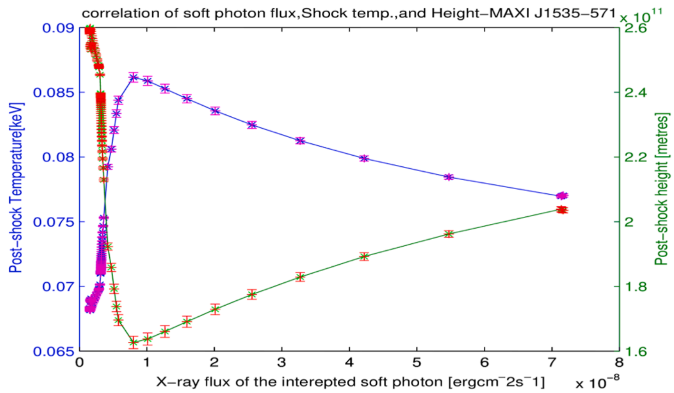

Fig. 9. Correlation shock temperature (Ts) and shock height (Hs) vs intercepted soft X-ray flux obtained using "*M7*"–fitted parameter. The data is asterisk (*; Ts is blue, Hs is green) whereas the error associated with each data point is the solid magenta and red cross with cap respectively.

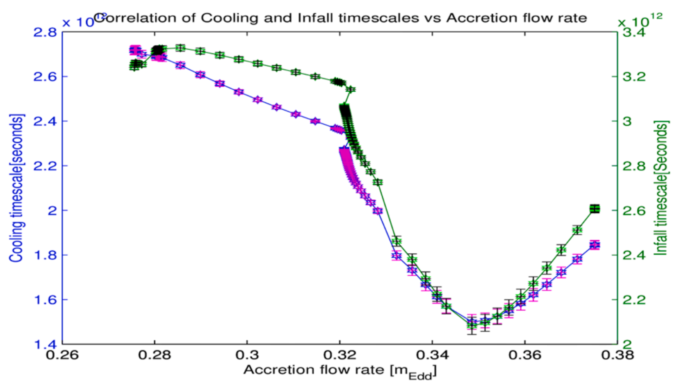

Fig. 10. Correlation of Cooling timescale (t_c) and Infall timescale (t_i) vs Accretion flow rate [m_{dot} $(d + h)$] obtained using "*M7*"–fitted parameters. The data is hexagram (t_c is blue, t_i is green) whereas the error associated with each data point is the solid magenta and black cross with cap respectively.

2013, 2014; references therein). Contrarily, the reverse is the case here. Hs and Ts are anti-correlated. This is an irregular pattern that suggests intermittent/ flickering behavior because the interception of soft photons adversely affects and changes the shape of the post-shock region periodically, causing X-ray flux variability, and spectral evolution (Ebisawa et al., 1993, 1994; Chakrabarti and Titarchuk, 1995; Esin et al., 1997; Homan et al., 2001; Gierlinski and Done, 2004; Homan and Belloni, 2005; Nnadi et al., 2012; Debnath et al., 2014, 2018; Tao et al., 2018; Nakahira et al., 2018). Therefore, accretion flow rate [$m_{dot}(d + h)$], and variations/fluctuation in other accretion flow characteristics/parameters depend on the variations/fluctuations of accretion flow intrinsic properties; $m_{dot}d$ and $m_{dot}h$. Hence, independent variations/fluctuations of $m_{dot}d$ and $m_{dot}h$ could directly and/or indirectly regulate the variation/fluctuations of other accretion flow characteristics, and perhaps, spectral evolution.

CRediT authorship contribution statement

Ambrose C. EZE: Writing – original draft, Project administration, Methodology, Formal analysis, Conceptualization. **Romanus N.C. EZE:** Writing – review & editing, Supervision, Methodology, Investigation, Formal analysis. **Augustine E. CHUKWUDE:** Supervision.

Declaration of competing interest

The authors declare the following financial interests/personal relationships which may be considered as potential competing interests: Prof. R.N.C. Eze reports financial support and travel were provided by Japan Society for the Promotion of Science (JSPS) for sponsoring RNCE, at Ehime University, 2–5, Bunkyocho, Matsuyama, Ehime 790–8577, Japan, under JSPS Invitation Fellow (short term). Ambrose C. Eze reports financial support was provided by African Astronomical Society (AFAS). R.N.C. EZE reports a relationship with Japan Society for the Promotion of Science (JSPS) for sponsoring RNCE, at Ehime University, 2–5, Bunkyocho, Matsuyama, Ehime 790–8577, Japan, under JSPS Invitation Fellow that includes: funding grants and travel reimbursement. Ambrose C. EZE reports a relationship with African Astronomical Society (AFAS) that includes: funding grants. The corresponding author is Eze A. C., Department of Geosciences, Godfrey Okoye University Enugu State, Nigeria. Email: jerry410001@gmail.com, Whatsapp/voice call number: +2,348,062,111,865.

This research work was done collectively by three authors; Ambrose Chukwudi EZE (the lead and corresponding author), Romanus N. C. EZE (Lead supervisor) & A. E. CHUKWUDE(Supervisor). A. C. Eze is a Ph.D student of Department of Physics and Astronomy, University of Nigeria Nsukka (UNN), but work as a Physics Lecturer in Godfrey Okoye University Enugu. Prof. Romanus N. C. EZE, & Prof. A. E. CHUKWUDE are Professors of Physics/staff of the Department of Physics and Astronomy, UNN. This manuscript is an extract from my Ph.D Thesis. The data reduction/analysis was collectively done by Eze A. C. and Prof. Romanus N. C. EZE. The spectral fitting/modeling and scientific writing was done by Eze A. C. whereas Prof. Romanus N. C. EZE. & Prof. A. E. CHUKWUDE supervise, proof read, make corrections, and give directives.

The authors do not have any competing interest on financial and/or non-financial issue, and otherwise.

However, the authors humbly solicit for the article publication charge (APC) be waived for us. This is because we were not able to secure sponsors; both from our employer and Nigeria federal government establishments or agencies, for this publication.

Thanks. If there are other authors, they declare that they have no known competing financial interests or personal relationships that could have appeared to influence the work reported in this paper.

Data availability

https://heasarc.gsfc.nasa.gov/docs/archive.htm.

Acknowledgment

We are grateful to the Japan Society for the Promotion of Science (JSPS) for sponsoring RNCE, at Ehime University, 2–5, Bunkyocho, Matsuyama, Ehime 790–8577, Japan, under JSPS Invitation Fellow (short term) where this project was initiated and *Swift/BAT, MAXI/GSC*, and *NuSTAR* observation team for providing data and relevant files used in the analysis presented here. We also acknowledge the useful discussions and assistance of Megumi Shidatsu in the analysis of data used in the paper. Also, ACE is grateful for the financial assistance of the African Astronomical Society (AFAS) towards this research. Opinions expressed and conclusions arrived at are those of the author and are not necessarily to be attributed to AfAS. www.africanastronomicalsociety.org. We are also grateful to Dipak Debnath of the Institute of Astronomy, Space and Earth Science, India for providing us the *TCAF* model and his guidance and assistance.

References

Banerjee, A., Bhattacharjee, A., Debnath, D., Chakrabarti, S.K., 2020. Spectral analysis of χ class data of GRS 1915+105 using TCAF solution. RAA 20 (12), 208. https://doi.org/10.1088/1674-4527/20/12/208, 202010pp.

Belloni, T.M., 2009. States and transitions in black-hole binaries. Lect. Notes Phys. 794, 53–84. https://doi.org/10.1007/978-3-540-76937-8_3. http://arxiv.org/abs/0909.2474v1.

Beloborodov, A.M., 1998. Plasma ejection from magnetic flares and the X-ray spectrum of Cygnus X-1. ApJ 510 (2), L123.

Bhargava, Y., Belloni, T., Bhattacharya, D., Misra, R., 2019. Spectro-timing analysis of MAXI J1535−571 using AstroSat. MNRAS 000 (0000), 1–7.

Blandford, R.D., Payne, D.G., 1981. Compton scattering in a converging fluid flow–II. Radiation-dominated shock. Mon. Not. R. Astron. Soc. 194 (4), 1041–1055.

Borozdin, K., Revnivtsev, M., Trudolyubov, S., Shrader, C., Titarchuk, L., 1999. Do the spectra of soft X-ray transients reveal bulk-motion inflow phenomenon? ApJ 517, 67–380.

Casella, P., Belloni, T., Homan, J., Stella, L., 2004. A study of the low-frequency quasi-periodic oscillations in the X-ray light curves of the black hole candidate XTE J1859 + 226. Astron. Astrophys. 426 (2), 587–600.

Chakrabarti, S.K., 1989. Standing shocks in isothermal rotating winds and accretion. Mon. Not. R. Astron. Soc. 240 (1), 7–21.

Chakrabarti, S.K., 1997. Spectral properties of accretion disks around black holes. II. Sub-Keplerian flows with and without shocks. Astrophys. J. 484 (1), 313.

Chakrabarti, S.K., 2015. Recent trends in the study of compact objects (RETCO-II): theory and observation. ASI Conference Series 12, 1, 2015–??

Chakrabarti, S.K., Mandal, S., 2006. The spectral properties of shocked two-component accretion flows in the presence of synchrotron emission. ApJ 642, L49–L52.

Chakrabarti, S.K., Manickam, S.G., 2000. Correlation among quasi-periodic oscillation frequencies and quiescent-state duration in black hole candidateGRS1915+ 105. ApJ 531 (1), L41.

Chakrabarti, S.K., Mondal, S., Debnath, D., 2015. Resonance condition and low-frequency quasi-periodic oscillations of the outbursting source H1743− 322. MNRAS 452 (4), 3451–3456.

Chakrabarti, S.K., & Titarchuk, L.G. (1995). Spectral properties of accretion disks around galactic and extragalactic black holes. *arXiv preprint astro-ph/9510005*.

Chauhan, J., Miller-Jones, J.C.A., Anderson, G.E., et al., 2019. An H I absorption distance to the black hole candidate X-ray binary MAXI J1535–571. MNRAS 000, 1–5.

Cúneo, V.A., Alabarta, K., Zhang, L., Altamirano, D., Méndez, M., Armas Padilla, M., Basak, A, 2020. A NICER look at the state transitions of the black hole candidate MAXI J1535− 571 during its reflares. MNRAS 496 (2), 1001–1012.

Debnath, D., Chakrabarti, S.K., Mondal, S., 2014. Implementation of two-component advective flow solution in xspec. MNRAS: Lett. 440 (1), L121–L125.

Debnath, D., Chakrabarti, S.K., Nandi, A., 2013. Evolution of the temporal and the spectral properties in 2010 and 2011 outbursts of H 1743-322. Adv. Space Res. 52 (12), 2143–2155.

Debnath, D., Jana, A., Chakrabarti, S.K., Chatterjee, D., Mondal, S., 2017. Accretion flow properties of swift J1753. 5-0127 during its 2005 outburst. Astrophys. J. 850 (1), 92.

Done, C., Gierliński, M., Kubota, A., 2007. Modelling the behaviour of accretion flows in X- ray binaries: everything you always wanted to know about accretion but were afraid to ask. Astron. Astrophys. Rev. 15, 1–66.

Dunn, R.J.H., Fender, R.P., Körding, E.G., Cabanac, C., Belloni, T., 2008. Studying the X-ray hysteresis in GX 339− 4: the disc and iron line over one decade. Mon. Not. R. Astron. Soc. 387 (2), 545–563.

Ebisawa, K., Makino, F., Mitsuda, K., Belloni, T., Cowley, A.P., Schmidtke, P.C., Treves, A., 1993. Spectral variations of LMC X-3 observed with GINGA. Astrophys. J. Part 1 403 (2), 684–689 (*ISSN 0004-637X), vol. 403684-689*.

Ebisawa, K., Mitsuda, K., Hanawa, T., 1991. Application of a general relativistic accretion disk model to LMC X-1, LMC X-3, X1608-522, and X1636-536. ApJ 367, 213–220.

Ebisawa, K., Ogawa, M., Aoki, T., Dotani, T., Takizawa, M., Tanaka, Y., Yosida, K., Miyamoto, S., Iga, S., Hayamoto, S., Kitamoto, S., Terada, K., 1994. Spectral evolution of the bright X-ray nova GS 1124-68 (Nova MUSCAE 1991) observed with GINGA. PASJ: Publications of the Astronomical Society of Japan 46 (4), 375–394 (*ISSN 0004-6264*), vol. 46*375-394*.

Esin, A.A., McClintock, J.E., &Narayan, R., 1997. Advection-dominated accretion & the spectral states of black hole X-ray binaries: application to nova MUSCAE1991. ApJ 489, 865–889.

Esin, A.A., Narayan, R., Cui, W., Grove, J.E., Zhang, S.N., 1998. Spectral transitions in cygnus X-1 and other black hole X-ray binaries. ApJ 505 (2), 854.

Esin, A.A., Narayan, R., Ostriker, E., & Yi, I. (1996). Hot one-temperature accretion flows around black holes. arXiv preprint astro-ph/9601074.

Galeev, A.A., Rosner, R., Vaiana, G.S., 1979. Structured coronae of accretion disks. ApJ 229, 318–326.

Gierlinaski, M., Zdziarski, A.A., Poutanen, J., Coppi, P.S., Ebisawa, K., Johnson, W.N., 1999. Radiation mechanisms and geometry of Cygnus X-1 in the soft state. MNRAS 309, 496–512.

Gierliński, M., Done, C., 2004. Black hole accretion discs: reality confronts theory. Mon. Not. R. Astron. Soc. 347 (3), 885–894.

Gierliński, M., Newton, J., 2006. X-ray spectral transitions of black holes from RXTE All-Sky Monitor. Mon. Not. R. Astron. Soc. 370 (2), 837–844.

Homan, J., Belloni, T., 2005. The evolution of black hole states. Astrophys. Space Sci. From X-Ray Binaries Quasars Black Holes Mass Scales 107–117.

Homan, J., Wijnands, R., van der Klis, M., Belloni, T., van Paradijs, J., Klein-Wolt, M., Fendr, R., Mendez, M., 2001. Correlated X-ray spectral and timing behavior of the black hole candidate XTE J1550–564: a new interpretation of black hole states. Astrophys. J. Supplem. Ser. 132 (2), 377.

Hua, X.M., Titarchuk, L., 1995. Comptonization models and spectroscopy of X-Ray and Gamma-Ray sources: a combined study by Monte Carlo and analytical methods. ApJ 449, 188, 449,*188*.

Ingram, A., Done, C., 2011. A physical model for the continuum variability and quasi-periodic oscillation in accreting black holes. MNRAS 415 (3), 2323–2335.

Iyer, N., Nandi, A., Mandal, S., 2015. Determination of the mass of IGR J17091–3624 from "Spectro-temporal" variations during the onset phase of the 2011 outburst. ApJ 807 (1), 108.

Kubota, A., Makishima, K., 2004. The three spectral regimes found in the stellar black hole XTE J1550–564 in its high/soft state. Astrophys. J. 601 (1), 428.

Kubota, A., Tanaka, Y., Makishima, K., Ueda, Y., Dotani, T., Inoue, H., Yamaoka, K., 1998. Evidence for a black hole in the X-ray transient GRS 1009-45. PASJ 50, 667–673.

Laurent, P., Titarchuk, L., 1999. The converging inflow spectrum is an intrinsic signature for a black hole: Monte Carlo simulations of Comptonization on free-falling electrons. ApJ 511 (1), 289.

Mandal, S., Chakrabarti, S.K., 2010. On the evolution of accretion rates in compact outburst sources. Astrophys. J. Lett. 710 (2), L147.

Méndez, M., van der Klis, M., 1997. The EXOSAT data on GX 339–4: further evidence for an "intermediate" state. ApJ 479 (2), 926–932.

Mereminskiy, I.A., Grebenev, S.A., Prosvetov, A.V., & Semena, A.N., (2018), Low frequency quasi-periodic oscillations in the X-ray Nova MAXI J1535-571 at the initial stage of its 2017 outburst. http://arxiv.org/abs/1806.06025v1.

Mikashima, K., Maejima, Y., Mitsuda, K., Bradt, H.V., Remillard, R.A., Tuohy, I.R., Hoshi, R., Nakagawa, M., 1986. Simultaneous X-ray and optical observations of GX 339-4 in an X- ray high state. ApJ 308, 635–643.

Mineshige, S., Wheeler, J.C., 1989. Disk-instability model for soft-X-ray transients containing black holes. ApJ 343, 241–253. Research supported by NSF., 343*, 241-253*.

Mitsuda, K., et al., 1984. Energy spectra of low-mass binary X-ray sources observed from TENMA. PASJ 36, 741–759.

Miyamoto, Sigenori, Kimura, Kazuhiro, Kitamoto, Shunji, Dotani, Tadayasu, Ebisawa, Ken, 1991. X- ray variability of GX 339-4 in its very high state. ApJ 383, 784–807.

Molla, A.A., Chakrabarti, S.K., Debnath, D., Mondal, S., 2017. Estimation of mass of compact object in H 1743-322 from 2010 to 2011 outbursts using TCAF solution and spectral index–QPO frequency correlation. Astrophys. J. 834 (1), 88.

Molla, A.A., Debnath, D., Chakrabarti, S.K., Mondal, S., Jana, A., 2016. Estimation of the mass of the black hole candidate MAXI J1659− 152 using TCAF and POS models. Mon. Not. R. Astron. Soc. 460 (3), 3163–3169.

Molteni, D., Sponholz, H., Chakrabarti, S.K., 1996. X-rays from shock waves in accretion flows around black holes. Roentgenstrahlung Universe 657–658.

Molteni, D.M., Sponholz, H., & Chakrabarti, S.K. (1995). Resonance oscillation of radiative shock waves in accretion disks around compact objects. *arXiv preprint astro-ph/9508022*.

Motta, S., Homan, J., Munoz-Darias, T., Casella, P., Belloni, T.M., Hiemstra, B., Méndez, M., 2012. Discovery of two simultaneous non-harmonically related quasi-periodic oscillations in the 2005 outburst of the black hole binary GRO J1655− 40. MNRAS 427 (1), 595–606.

Nakahira, S., Shidatsu, M., Makishima, K., et al., (2018), Discovery and state transitions of the new Galactic black hole candidate MAXI J1535 − 571. http://arxiv.org/abs/1804.00800v2.

Nandi, A., Debnath, D., Mandal, S., Chakrabarti, S.K., 2012. Accretion flow dynamics during the evolution of timing and spectral properties of GX 339-4 during its 2010–11 outburst. A &A 542, A56.

Nandi, A., Mandal, S., Sreehari, H., Radhika, D., Das, S., Chattopadhyay, I., Iyer, N., Agrawal, V.K., Aktar, R., 2018. Accretion flow dynamics during 1999 outburst of XTEJ1859+226— Modeling of broadband spectra and constraining the source mass. Astrophys. Space Sci. 363, 90. https://doi.org/10.1007/s10509-018-3314-1.

Narayan, R., McClintock, J.E., & Yi, I. (1995). A new model for black hole soft X-ray transients in quiescence. *arXiv preprint astro-ph/9508014*.

Negoro, H., Ishikawa, M., Ueno, S., et al., 2017a. MAXI/GSC discovery of a new hard X-ray transient MAXI J1535-571. Astronomer's Telegr. 10699.

Negoro, H., Kawase, T., Sugizaki, M., et al., 2017b. Further Brightening of the X-ray Transient MAXI J1535-571, Suggesting the Presence of a Black Hole. Astronomer's Telegram, p. 10708.

Parikh, A.S., Russell, T.D., Wijnands, R., et al., (2019), Rapidly evolving disk-jet coupling during re-brightenings in the black hole transient MAXI J1535−571. http://www.aiXiv:1906.01000v2.

Parikh, A.S., Russell, T.D., Wijnands, R., Bahramain, A., Miller-Jones, J.C.A., Tetarenko, A.J., Sivakoff, G.R., 2018. *Re*-brightening of the black hole candidate MAXI J1535-571 as it transitioned back to the soft state. Astronomer's Telegr. 11652, 1.

Remillard, R.A., McClintock, J.E., 2006. X-ray properties of black-hole binaries. Annu. Rev. Astron. Astrophys. 44, 49–92.

Ryu, D., Chakrabarti, S.K., Molteni, D., 1997. Zero-energy rotating accretion flows near a black hole. ApJ 474 (1), 378.

Shang, J.R., Debnath, D., Chatterjee, D., Jana, A., Chakrabarti, S.K., Chang, H.K., Yap, Y.-X, Chiu, C.L., 2019. Evolution of X-ray Properties of MAXI J1535-571: analysis with the TCAF Solution. ApJ 875 (1), 4.

Shidatsu, M., Ueda, Y., Yamada, S., et al., 2014. Spectral and Timing properties of the blackhole X-ray binary H1734 -322 in the low/hard state studied with Suzaku. ApJ 789, 100. https://doi.org/10.1088/0004-637X/789/2/100.

Shimura, T., Takahara, F., 1995. On the spectral hardening factor of the X-ray emission from accretion disks in blackhole candidates. ApJ 445, 780–788.

Sreehari, H., Ravishankar, B.T., Iyer, N., Agrawal, V.K., Katoch, T.B., Mandal, S., Nandi, A., 2019. AstroSat view of MAXI J1535−571: broadband spectro-temporal features. MNRAS, 000, 1–15.

Stiele, H., Kong, A.K.H., 2018. A spectral and timing study of MAXI J1535–571, based on swift/XRT, XMM-newton, and NICER observations obtained in fall 2017. ApJ 868 (1), 71.

Sunyaev, R.A., Titarchuk, L.G., 1980. Comptonization of X-rays in plasma clouds-Typical radiation spectra. A &A 86, 121–138.

Sunyaev, R.A., Truemper, J., 1979. Hard X-ray spectrum of CYG X-1. Nature 279 (5713), 506–508.
Tanaka, Y., Shibazaki, N., 1996. X-ray Novae. Ann. Rev. of A& A 34 (1), 607–644.
Tao, L., Chen, Y., Güngör, C., Huang, Y., Lu, F., Qu, J., Song, L., Zhang, L., Zhang, S., Zhang, S., 2018. Swift observations of the bright uncatalogued X-ray transient MAXI J1535-571. MNRAS 480 (4), 4443–4454.
Titarchuk, L., 1994. Generalized comptonization models and application to the recent high energy observations. In: AIP Conference Proceedings, 304. American Institute of Physics, pp. 380–384.
Titarchuk, L., Mastichiadis, A., Kylafis, N.D., 1997. X-ray spectral formation in a converging fluid flow: spherical accretion into blackholes. ApJ 487, 834–846.
Titarchuk, L., & Seifina, E., (2016), Scaling of the photon index vs mass accretion rate correlation and estimate of black hole mass in M101 ULX-1. http://de.arxiv.org/abs/1510.06978v1.
Titarchuk, L., Seifina, E., Chekhtman, A., Indira, O., 2020. Spectral index − mass accretionrate correlation and evaluation of black hole masses in AGNs 3C 454.3 and M 87. A&A 633, A73. https://doi.org/10.1051/0004-6361/201935576.
Titarchuk, L., Shaposhnikov, N., Arefiev, V., 2007. Power spectra of black holes and neutron stars as a probe of hydrodynamic structure of the source: diffusion theory and its application to Cygnus X-1 and Cygnus X-2 X-ray observations. Astrophys. J. 660 (1), 556.
Titarchuk, L., Zannias, T., 1998. The extended power law as an intrinsic signature for a black hole. ApJ 493 (2), 863.
Trudolyubov, S., Gilfanov, M., Churazov, E., Sunyaev, R., Khavenson, N., Dyachkov, A., Tserenin, I., Sukhanov, K., Laurent, P., Ballet, J., Goldoni, P., Paul, J., Roques, J-P., Borrel, V., Bouchet, L., Jourdain, E., 1998. Hard X-ray observations of GX 339-4 with GRANAT/SIGMA. A&A 334, 895–900.
Vignarca, F., Migliari, S., Belloni, T., Psaltis, D., Van Der Klis, M, 2003. Tracing the power- law component in the energy spectrum of black hole candidates as a function of the QPO frequency. A &A 397 (2), 729–738.
Xu, Y.A., Harrison F.A., and Garcia, J.A., (2018), Reflection Spectra of the blackhole candidate MAXI J1535-571 in the hard state observed by NUSTAR. http://arxiv.org/abs/1711.01346v2.
Yaqoob, T., 1997. X-ray transmission in cold matter: nonrelativistic corrections for compton scattering. Astrophys. J. 479 (1), 184.
Życki, P.T., Done, C., Smith, D.A., 1999. The 1989 May outburst of the soft X-ray transient GS 2023+ 338 (V404 Cyg). Mon. Not. R. Astron. Soc. 309 (3), 561–575.